

1 **Evaluation of Arctic sea ice thickness simulated by AOMIP models**

2 Mark Johnson¹, Andrey Proshutinsky², Yevgeny Aksenov³, An T. Nguyen⁴, Ron Lindsay⁵,
3 Christian Haas⁶, Jinlun Zhang⁵, Nikolay Diansky⁷, Ron Kwok⁸, Wieslaw Maslowski⁹, Sirpa
4 Hakkinen¹⁰, Igor Ashik¹¹, Beverly de Cuevas³.

5 ¹*Institute of Marine Science, University of Alaska Fairbanks, Fairbanks, AK, USA*

6 ²*Wood Hole Oceanographic Institution, Woods Hole, MA, US*

7 ³*National Oceanography Centre, Southampton, Southampton, UK*

8 ⁴*Massachusetts Institute of Technology, Cambridge, MA, USA*

9 ⁵*Polar Science Center, University of Washington, Seattle, WA, USA*

10 ⁶*University of Alberta, Edmonton, Canada*

11 ⁷*Institute of Numerical Mathematics Russian Academy of Sciences, Moscow, Russia*

12 ⁸*Jet Propulsion Laboratory, Pasadena, CA, USA*

13 ⁹*Naval Postgraduate School, Monterey, CA, USA*

14 ¹⁰*Goddard Space Flight Center, Greenbelt, MD, USA*

15 ¹¹*Arctic and Antarctic Research Institute, St. Petersburg, Russia*

16 **Abstract**

17 We compare results from six AOMIP model simulations with estimates of sea ice thickness
18 obtained from ICESat, moored and submarine-based upward looking sensors, airborne
19 electromagnetic measurements and drill holes. Our goal is to find patterns of model performance
20 to guide model improvement. The satellite data is pan-arctic from 2004–2008, ice-draft data is
21 from moored instruments in Fram Strait, the Greenland Sea and the Beaufort Sea from 1992–
22 2008 and from submarines from 1975-2000. The drill hole data are from the Laptev and East
23 Siberian marginal seas from 1982–1986 and from coastal stations from 1998-2009. While there
24 are important caveats when comparing modeled results with measurements from different
25 platforms and time periods such as these, the models agree well with moored ULS data. In
26 general, the AOMIP models underestimate the thickness of measured ice thicker than about 2 m
27 and overestimate thickness of ice thinner than 2 m. The simulated results are poor over the fast
28 ice and marginal seas of the Siberian shelves. Averaging over all observational data sets, the
29 better correlations and smaller differences from observed thickness are from the ECCO2 and
30 UW models.

31 **1. Introduction**

32 Dramatic decreases in Arctic sea ice are predicted by some climate models to the degree that
33 multiyear ice may be lost during this century. Critical to the accuracy and reliability of high
34 latitude climate forecasts and a better understanding of sea ice dynamics and thermodynamics is
35 the proper simulation of sea ice and its responses to atmospheric forcing across a range of
36 temporal and spatial scales. Assessment of model performance regarding sea ice would include,
37 at least, comparisons with observations of the interrelated sea ice characteristics of motion,
38 strain, deformation, concentration, age, and thickness. Evaluation of modeled sea ice behavior,

39 however, is limited by incomplete observational data across the scales that characterize sea ice
40 growth, melt, motion, and divergence.

41 With the beginning of the satellite record in the late 1970s, sea ice concentration became
42 widely available as a product derived from passive microwave brightness temperatures
43 [Gloersen *et al.*, 1992]. However, estimating sea ice thickness is not straightforward although
44 procedures for estimating thickness as well as velocity from the satellite record have been
45 developed [Laxon *et al.*, 2003; Kwok *et al.*, 2004]. Thickness is important to estimates of sea ice
46 survival probability over the melt season [Untersteiner, 1961] and its distribution appears to be
47 undergoing rapid changes [Wadhams, 1990; Rothrock *et al.*, 1999; Wadhams and Davis, 2000].

48 The focus of this paper is on the ability of six coupled Arctic Ocean Model Intercomparison
49 Project (AOMIP) models to simulate sea ice thickness and to identify trends and differences
50 among the AOMIP model ice thickness results by comparing them with the broad range of
51 observed sea ice thickness data that is now available. The observational data include a) gridded
52 ice thickness derived from the ICESat satellite for ten campaigns from fall and winter 2004
53 through 2008, b) ice thickness transect data from electromagnetic airborne measurements (2001-
54 2009), c) ice draft from 24 moored instruments equipped with upward looking sonars (ULS) and
55 ice profiling sonars (IPS) from 1992 through 2008 from the Beaufort Sea, Fram Strait and the
56 Greenland Sea, d) ice draft from submarines equipped with upward-looking sonar (1975-2000),
57 e) ice thickness in drill-holes through sea ice from 187 sites taken in spring from 1982 through
58 1986 across the Siberian marginal seas, and f) fast ice thickness from 51 Russian coastal stations
59 (1998-2009). As described below, all ice-draft data were converted to ice thickness.

60 For this paper a range of thickness measurements is important to assess model performance.
61 When and where ice is thin and/or in low concentration there is potential for high speed drift that

62 may lead to dynamically driven increases in thickness via deformation while at the same time
63 provide the potential for ice growth thermodynamically. Therefore, it is important to know
64 whether specific models perform differently when simulating “thin” versus “thick” sea ice.

65 Because of differences among model forcing, processes, and parameterizations even within a
66 coordinated modeling project such as AOMIP, our goal here is to identify the agreement between
67 modeled sea ice and observations in order to provide a foundation for model improvement.
68 However, the complexity of isolating specific model attributes from among the full suite of
69 parameterizations, forcing, and boundary conditions is beyond the scope of this paper. In the end,
70 the utility of comparisons such as those done here may be assessed by the rate of model
71 improvement.

72 2. Summary of previous work

73 *Bourke and Garrett* [1987] first reported on the mean ice thickness distribution in the Arctic
74 Ocean from data taken between 1960 and 1982. *Rothrock et al.* [1999] showed that that the
75 mean ice draft in most of the central portion of the Arctic Ocean had declined from 3.1 m in
76 1958–1976 to 1.8 m in the 1990s (a 40% decrease). The submarine ice draft data in the data
77 release area (DRA) were fit with multiple linear regression expressions of location, time and
78 season by *Rothrock et al.* [2008] for the period 1975–2000. They found the annual mean ice draft
79 declined from a peak of 3.42 m in 1980 to a minimum of 2.29 m in 2000. ICESat ice thickness
80 estimates for 2003–2008 for the same area of the Arctic Ocean as represented by the regression
81 equations match well with the earlier submarine records [*Kwok and Rothrock*, 2009] and show a
82 continued decline to less than 1.0 m in the DRA in the fall of 2007. *Wadhams and Davis* [2000]
83 also found a decline in the ice draft at the pole of 43% from 1976 to 1996. *Winsor* [2001],
84 however, found no trend in six cruises between the pole and the Beaufort Sea from the 1990’s.

85 Airborne EM surveys by *Haas et al.* [2009] showed a thinning of 20% in the region of the North
86 Pole between 1991 and 2004, with a sharp drop to only 0.9 m in the summer of 2007 related to
87 the replacement of old ice by first-year ice.

88 Direct comparison of model results to observed sea ice thickness has been limited because
89 pan-Arctic sea ice thickness data were not widely available at useful resolutions. The lack of
90 observational data was carefully circumvented by *Gerdes and Koberle* [2007] who compared
91 results from several IPCC modeled outputs against sea ice thickness from a hindcast model
92 (AWI1) positively evaluated against other AOMIP models. They concluded that differences
93 among the IPCC models were likely due to the different effective wind stress forcing and the
94 coupling methodologies with the ocean, a conclusion consistent with studies showing that
95 atmospheric forcing fields essentially drive the results of sea ice simulations [*Walsh and Crane,*
96 *1992; Bitz et al., 2002; Hunke and Holland, 2007*] more so than the details of the sea ice model
97 itself [*Flato et al., 2004*].

98 For sea ice concentration, satellite-derived values were compared with several AOMIP
99 models to show that they reproduced winter-time observations reasonably well when ice
100 concentration was near 100% but underestimated the September ice concentration minimum
101 [*Johnson et al., 2007*]. The variability among model results exceeded the variability among four
102 satellite-derived observational data sets suggesting the need to further constrain model
103 performance or reduce sensitivity to prescribed forcing.

104 Assessment of model performance using sea ice drift and deformation derived from satellite
105 data indicates little agreement between modeled patterns of sea-ice deformation fields and the
106 linear features produced from the RADARSAT Geophysical Processor System (RGPS) at days
107 to seasons and from kilometers to near basin scale [*Kwok, et al., 2008*]. Compared to the RGPS

108 products, specific model shortcomings included slow ice drift along coastal Alaska and Siberia,
109 poor temporal rates of regional ice cover divergence, and low deformation-related ice volume
110 production.

111 Assessment of the ice age-thickness relationship using model results shows that for northern
112 hemisphere-wide averages the notion of thicker ice being older is reasonable at decadal scales,
113 but for specific years and at scales less than hundreds of kilometers, ice age is not a good proxy
114 for ice thickness [*Hunke and Bitz, 2009*]. At interannual time scales, the northern hemisphere
115 averaged ice age is not well correlated with any of the three common ice descriptors: thickness,
116 area or volume.

117 This paper is organized as follows. In the next section we present the six different AOMIP
118 models followed by a review of the data sets against which they are compared. A section on the
119 methods used to prepare the model and observational data follow. Comparison between models
120 and data use a Taylor diagram modified to retain units of ice thickness residuals and model-data
121 correlations, and also examines the linear regressions between the model and observed data. The
122 paper concludes with a discussion of options for model improvement and a summary.

123 3. Models

124 The AOMIP project and its models were described previously in *Holland et al.* [2007] with
125 considerable detail to be found on the AOMIP web site [<http://www.whoi.edu/projects/AOMIP>].
126 The six models used are from the Goddard Space Flight Center (GSFC), Jet Propulsion
127 Laboratory (Estimating the Circulation and Climate of the Ocean, Phase II -- ECCO2), Institute
128 of Numerical Mathematics Ocean Model (INMOM) Russian Academy of Science, the National
129 Oceanography Centre Southampton (ORCA), the Naval Postgraduate School (NPS) Arctic

130 Modeling Effort (NAME), and the University of Washington (UW). Specific sea ice parameters
131 for these models are shown in Table 1

132 3.1 GSFC

133 The GSFC model is based on the generalized Princeton Ocean Model (POM) which can
134 accommodate sigma-coordinates (the original POM), but also z-levels and a mixture of sigma
135 and z-levels, as the vertical coordinate [*Blumberg and Mellor, 1987; Mellor et al. 2002*]. The
136 results presented here are from a version which uses only z-levels. The vertical mixing
137 coefficients are determined from 2.5 layer turbulence closure (*Mellor and Yamada, 1974*) which
138 requires computation of the kinetic energy and kinetic energy times mixing length as additional
139 prognostic quantities. The ocean model is coupled to a two-layer dynamic- thermodynamic
140 snow-ice model where the sea ice is described as a generalized viscous medium [*Mellor and*
141 *Kantha, 1989; Hakkinen and Mellor, 1992; Hakkinen and Geiger, 2000*]. Ice-ocean momentum,
142 heat and salt exchange is described by a flow over a rough surface based on the theory of *Yaglom*
143 *and Kader* [1974]. The solar radiation can penetrate below the ocean surface to distribute short-
144 wave solar heating.

145 The model domain covers the Arctic Ocean and the North Atlantic and extending to 15°S,
146 with a horizontal resolution of 0.35-0.45 degrees. Vertical resolution is 26 levels ranging from
147 6m to 500m layer depths. Transport at the open boundaries is defined by an inflow of 0.8 Sv
148 through Bering Strait, which equals the amount that exits through the model's southern boundary
149 at approximately 15°S. The monthly T and S are restored at the open boundary buffer zones, but
150 no other restoring is used in the GSFC model.

151 The specifications for AOMIP coordinated model run forcing are adopted except the
152 following: P-E from *Rasmusson and Mo* [1996], and the Sellers formula as in *Parkinson and*

153 *Washington* [1979] for short wave radiation instead of AOMIP recommendations; the model uses
154 NCEP wind stress instead of AOMIP recommended wind forcing. The GSFC model results are
155 from a cold start at January 1948 using daily NCEP Reanalysis data.

156 3.2 ECCO2

157 The Arctic domain of ECCO2 uses a regional configuration of the Massachusetts Institute of
158 Technology general circulation model (MITgcm, [*Marshall et al.*, 1997; *Losch et al.*, 2010,
159 *Nguyen et al.*, 2011]). The domain has southern boundaries at $\sim 55^\circ\text{N}$ in the Atlantic and Pacific
160 sectors. The grid is locally orthogonal with horizontal grid spacing of approximately 18 km.
161 There are 50 vertical levels ranging in thickness from 10 m near the surface to approximately
162 450 m at a maximum model depth of 6150 m. The model employs the rescaled vertical
163 coordinate “z*” of *Adcroft and Campin* [2004] and the partial-cell formulation of *Adcroft et al.*
164 [1997], which permits accurate representation of the bathymetry. Bathymetry is from the S2004
165 (*W. Smith*, unpublished) blend of the *Smith and Sandwell* [1997] and the General Bathymetric
166 Charts of the Oceans (GEBCO) one arc-minute bathymetric grid. The non-linear equation of
167 state of *Jackett and McDougall* [1995] is used. Vertical mixing follows *Large et al.* [1994]. A
168 7th-order monotonicity-preserving advection scheme [*Daru and Tenaud*, 2004] is employed and
169 there is no explicit horizontal diffusivity. Horizontal viscosity follows *Leith* [1996] but is
170 modified to sense the divergent flow [*Fox-Kemper and Menemenlis*, 2008].

171 The ocean model is coupled to the MITgcm sea ice model described in *Losch et al.* [2010].
172 Ice mechanics follow a viscous-plastic rheology and the ice momentum equations are solved
173 numerically using the line-successive-over-relaxation (LSOR) solver of *Zhang and Hibler*
174 [1997]. Ice thermodynamics are represented using a zero-heat-capacity formulation and seven
175 thickness categories. Salt rejection during sea-ice formation is explicitly treated with a subgrid

176 salt plume parameterization [Nguyen *et al.*, 2009]. The model includes prognostic variables for
177 snow thickness and for sea ice salinity. Boundary conditions are monthly and taken from the
178 global optimized ECCO2 solution [Menemenlis *et al.*, 2008]. Initial conditions are from the
179 World Ocean Atlas 2005 [Antonov *et al.*, 2006; Locarnini *et al.*, 2006]. Atmospheric boundary
180 conditions are from the Japanese 25-year Reanalysis Project (JRA25, [Onogi *et al.*, 2007]. The
181 integration period is from 1992-2008. A comprehensive assessment of the solution used in this
182 study can be found in Nguyen *et al.* [2011] where the model solution is parameter optimized
183 from 1992 to 2004 using ice thickness data from submarine and mooring ULS, sea ice
184 concentration and velocity, and ocean hydrography.

185 3.3 INMOM

186 The INMOM is a “terrain following” sigma-coordinate ocean model [Moshonkin *et al.*, 2011].
187 The global version of the INMOM with low spatial resolution is used as the oceanic component
188 of the IPCC climate model INMOM [Volodin *et al.*, 2010] presented in the IPCC Fourth
189 Assessment Report [2007]. The present version of the model covers the North Atlantic (open
190 boundary at approximately 20°S), Arctic Ocean, and Bering Sea regions including
191 Mediterranean and Black Seas. A rotation of the model grid avoids the problem of converging
192 meridians over the Arctic Ocean. The model North Pole is located at the geographical equator,
193 120°W. The 1/4° horizontal eddy-permitting resolution is used. There are 27 unevenly spaced
194 vertical sigma-levels. A Laplacian operator along the geopotential surface is used for the lateral
195 diffusion on the tracers and a bilaplacian operator along sigma-surface is used for the lateral
196 viscosity on momentum. The vertical viscosity and diffusion coefficients are calculated by
197 Monin-Obuhov-Kochergin [Kochergin, 1987] parameterization. The elastic-viscous-plastic
198 (EVP) dynamic - thermodynamic sea ice model [Hunke, 2001; Yakovlev, 2009] is coupled to the

199 ocean model. Surface forcing is from the CORE forcing dataset [*Large and Yeager, 2004*]. The
200 surface turbulent fluxes are calculated using the bulk formulae. A climatological monthly runoff
201 from CORE is applied along the coasts. Surface salinity is restored towards monthly climatology
202 with a relaxation scale of approximately 12 days both for the open ocean and under sea-ice.
203 Temperature and salinity restoring towards monthly climatology is used at the open boundaries.

204 3.4 ORCA

205 The ORCA model is a global z-level OGCM based on the NEMO ocean code [*Madec, 2006*]
206 and uses the global tri-polar ORCA grid at $\frac{1}{4}^\circ$ horizontal resolution. The effective resolution is
207 ~ 27.75 km at the equator increasing to 6-12 km in zonal and ~ 3 km in meridional directions in
208 the Arctic Ocean, thus the model resolves large eddies in the Arctic Ocean and “permits” smaller
209 ones. The configuration was developed by the DRAKKAR project and is described by *Barnier et*
210 *al.* [2006] as the ORCA025-G70 configuration. The version of the model used here has a higher
211 vertical resolution (64 vertical levels) than the ORCA025-G70, with thicknesses of the model
212 levels ranging from ~ 6 m near the surface to ~ 204 m at 6000 m. The ‘partial step’ topography
213 [*Adcroft et al., 1997, Pacanowski & Gnanadesikan, 1998*] is used, whereby the bottom cell is
214 variable and more able to represent small topographic slopes near the Arctic shelves, resulting in
215 the more realistic along-shelf flow [e.g., *Barnier et al., 2006; Penduff et al., 2007*]. The ocean
216 model is coupled asynchronously to the sea ice model every five oceanic time steps through a
217 non-linear quadratic drag law [*Timmermann et al., 2005*].

218 The sea-ice model LIM2 [*Fichefet et al., 1997*] is based on the Viscous-Plastic (VP) rheology
219 with an elliptic yield curve [*Hibler, 1979*] and Semtner’s 2-layer ice, 1-layer snow
220 thermodynamics [*Semtner, 1976*]. The latter is updated with sea ice thickness distribution
221 [*Fichefet et al., 1997*]. Other features of the model are the positive-definite, second order, second

222 moments conserving advection scheme [Prather, 1986], ice-thickness dependent *albedo* [Payne,
223 1972), lateral ice thermodynamics and a simple snow-ice formation mechanism due to
224 hydrostatic imbalance [Fichefet et al., 1997]. Sea ice salinity is taken equal to 4, the average
225 value of sea ice salinity in the Central Arctic Ocean. Heat exchange between the ocean and sea
226 ice is calculated as a product from the departure of surface temperature from the salinity-
227 dependent freezing point and friction velocity at the ice-ocean interface. Solar radiation
228 penetrates snowless ice, increasing latent heat storage in brine pockets [Fichefet et al., 1997].

229 Surface forcing is provided by the DRAKKAR Forcing Set 3 [Brodeau et al., 2001]. This
230 dataset is a combination of precipitation and downward longwave and shortwave radiation fields
231 from the CORE forcing dataset [Large and Yeager, 2004] and 10-m wind, 2-m air temperature
232 and 2-m specific humidity from the ECMWF ERA40 re-analysis product. The turbulent air/sea
233 and air/ice fluxes are calculated by the model using the bulk formulae [Large and Yeager, 2004].
234 A climatological monthly runoff [Dai and Trenberth, 2002] is applied along the coasts. Surface
235 salinity is restored towards monthly climatology with a relaxation scale of 180 days for the open
236 ocean and 12 days under sea-ice.

237 3.5 Naval Postgraduate School (NPS) Arctic Modeling Effort (NAME)

238 The NPS pan-Arctic coupled ice-ocean model used in this study consists of a Hibler-type sea
239 ice model (Zhang and Hibler, 1997) coupled to a regional adaptation of the Parallel Ocean
240 Program (POP) [Smith et al., 1992; Smith and Gent, 2002]. The sea ice model employs a
241 viscous-plastic rheology, two ice thickness categories (mean ice thickness and open water), the
242 zero-layer approximation of heat conduction through ice and a simplified surface energy budget
243 (Zhang et al., 1999; Maslowski et al., 2000). The ice strength is parameterized in this model as a
244 function of the mean grid-cell ice thickness, which tends to underestimate ice drift and

245 deformation [Maslowski and Lipscomb, 2003; Kwok et al., 2008]. The ocean model is a z-
246 coordinate ocean model with an implicit free surface and 45 vertical levels, with layer thickness
247 ranging from 5 m near the surface to 300 m at depth.

248 The model domain includes all sea-ice covered oceans and marginal seas of the northern
249 hemisphere. It includes the Arctic Ocean, sub-Arctic seas and extends to $\sim 30^{\circ}\text{N}$ in the North
250 Pacific and to $\sim 45^{\circ}\text{N}$ in the North Atlantic. Both components of the coupled model use identical
251 horizontal grid configured at $1/12^{\circ}$ (~ 9 km) in a rotated spherical coordinate system to eliminate
252 the North Pole singularity. The model lateral boundaries are solid and no mass flux is allowed
253 through them however a virtual annual cycle salt flux is prescribed for most major rivers as a
254 function of river run-off. Surface layer (0-5 m) temperature and salinity are restored toward
255 monthly climatology [PHC; Steele et al., 2001]) on timescales of 365 and 120 days, respectively.

256 The model was forced with daily-average atmospheric fields (downward longwave and
257 shortwave radiation, surface air temperature, specific humidity, wind velocity and stress) from
258 the European Centre for Medium-range Weather Forecasts (ECMWF) 1979–1993 reanalysis and
259 1994-2004 operational products. Additional details of model configuration, initialization and
260 integrations can be found in Maslowski et al. [2004, 2008].

261 3.6 University of Washington (UW)

262 The UW model is the coupled pan-arctic ice–ocean modeling and assimilation system
263 (PIOMAS), a regional version of the global Parallel Ocean and Ice Model (POIM) [Zhang and
264 Rothrock, 2003]. The sea ice model is the multi-category thickness and enthalpy distribution
265 (TED) sea ice model [Zhang and Rothrock, 2001; Hibler, 1980]. It employs a teardrop plastic
266 rheology [Zhang and Rothrock, 2005], a mechanical redistribution function for ice ridging
267 [Thorndike et al., 1975; Hibler, 1980], and a LSR (line successive relaxation) dynamics model to

268 solve the ice momentum equation [Zhang and Hibler, 1997]. The TED ice model also includes a
269 snow thickness distribution model following Flato and Hibler [1995]. The ocean model is based
270 on the Parallel Ocean Program (POP) developed at Los Alamos National Laboratory [Smith et
271 al., 1992]. The model domain of PIOMAS covers the northern hemisphere north of 48°N. The
272 POP ocean model has been modified to incorporate open boundary conditions [Zhang and Steele,
273 2007] so that PIOMAS is able to be one-way nested to a global POIM [Zhang, 2005] with open
274 boundary conditions along 49°N. The PIOMAS finite-difference grid is based on a generalized
275 orthogonal curvilinear coordinate system with the “north pole” of the model grid placed in
276 Greenland. The model horizontal resolution ranges from 6 to 75 km with a mean resolution of 22
277 km for the Arctic, Barents, and GIN (Greenland-Iceland-Norwegian) seas, and Baffin Bay. The
278 TED sea ice model has 12 categories each for ice thickness, ice enthalpy, and snow depth. The
279 centers of the 12 ice thickness categories are 0, 0.26, 0.71, 1.46, 2.61, 4.23, 6.39, 9.10, 12.39,
280 16.24, 20.62, and 25.49 m. The POP ocean model has 30 vertical levels of varying thicknesses to
281 resolve surface layers and bottom topography. The first 13 levels are in the upper 100 m and the
282 upper six levels are each 5 m thick. The model bathymetry is obtained by merging the IBCAO
283 (International Bathymetric Chart of the Arctic Ocean) dataset and the ETOPO5 (Earth
284 Topography Five Minute Gridded Elevation Data Set) dataset [see Holland, 2000]. PIOMAS is
285 forced by daily NCEP/NCAR reanalysis [Kalnay et al., 1996] surface forcing fields, i.e., 10 m
286 surface winds, 2 m surface air temperature (SAT), specific humidity, precipitation, evaporation,
287 downwelling longwave radiation, sea level pressure, and cloud fraction. Cloud fraction and SAT
288 are used to calculate downwelling shortwave radiation following Parkinson and Washington
289 [1979]. Model forcing also includes river runoff of freshwater in the Arctic Ocean.
290 Climatological river runoff (i.e., no interannual variability) is provided as in the work of Hibler

291 *and Bryan* [1987]. The calculations of surface momentum and radiation fluxes follow *Zhang and*
292 *Rothrock* [2003] and differ from the specifications for the AOMIP coordinated runs. No climate
293 restoring is allowed. No data assimilation is performed for this study, although PIOMAS is able
294 to assimilate ice concentration and sea surface temperature data.

295 **4. Observational data**

296 Ice thickness from models is compared with observed thickness, ice draft or freeboard that has
297 been converted to thickness. Conversion for undeformed ice without snow or melt ponds is
298 straightforward. Assuming ice is in hydrostatic equilibrium with seawater, ice thickness is the
299 draft times the ratio of seawater density to sea-ice density. Snow cover, melt ponds and deformed
300 ice provide sources of error. Still, it is not uncommon to use thickness as the product of draft and
301 some constant. We use 1.115 [*Bourke and Paquette*, 1989] to convert draft to thickness.

302 Much of the data used in this study is available from the new Unified Sea Ice Thickness
303 Climate Data Record [*Lindsay*, 2010]. This archive has summary statistics for moorings,
304 submarines, aircraft, and satellite measurements of ice draft and ice thickness. The summary
305 statistics include mean, minimum, maximum, and standard deviation of the measurement as well
306 as the full probability density distribution. There are currently over 3000 samples in the archive
307 which can be accessed along with documentation and metadata at
308 http://psc.apl.washington.edu/sea_ice_cdr.

309 **4.1 ICESat campaigns**

310 Gridded Arctic Ocean sea ice thickness fields with resolution of 25 km \times 25 km (Figure 1a)
311 from 2004 through 2008 have been created from five fall and five winter ICESat campaigns
312 [*Kwok et al.*, 2009]. There is typically a three to four month separation between the fall and
313 winter campaigns. The duration, start and end dates of the fall and winter campaigns, shown in

314 Table 2, are variable. The five fall campaigns start between September 24th and October 25th and
315 end between November 8th and November 27th. Winter campaigns start between February 17th
316 and March 12th and end between March 21 and April 14th. We expect these shifts in the
317 individual satellite campaign timing to introduce seasonal and interannual variability within the
318 dataset, although it may not be particularly large as thicknesses represent near maximum end-of-
319 winter and minimum end-of-summer data.

320 The ICESat thickness data are derived from freeboard (distance above the water line to top of
321 the snow cover) obtained from the Geoscience Laser Altimeter System (GLAS). The
322 methodology for determining freeboard, snow depth, and ice thickness from the 70 m footprint
323 for ICESat is given by *Kwok et al.* [2007] and *Kwok et al.* [2009]. The empirical relationship
324 between thickness and freeboard for the first year (FY) ice in late winter is discussed in
325 *Alexandrov et al.* [2010].

326 Satellite grid point values were computed and a 50-km Gaussian smoothing applied. The
327 satellite hole is filled using an interpolation procedure described in *Kwok et al.* [2009]. ICESat
328 estimates [*Kwok et al.*, 2009] of ice drafts are consistently within 0.5 m (one standard deviation)
329 of profiles from a submarine cruise in mid-November of 2005, and four years of ice draft from
330 moorings (BGEP-WHOI and AIM-IOS) in the Chukchi and Beaufort Seas. The gridded ICESat
331 ice thickness estimates are available at the Jet Propulsion Laboratory at
332 <http://rkwok.jpl.nasa.gov/icesat/index.html>. The error variance of the ICESat thickness data is
333 (0.37 m^2) [*Kwok and Rothrock*, 2009]. The ICESat measurements, when converted to drafts, are
334 smaller on average by 0.1 ± 0.42 m than adjusted ULS submarine drafts (see Section 4.4) and by
335 0.14 ± 0.51 m than ULS moored drafts [*Kwok et al.*, 2009].

336 4.2 Electromagnetic airborne soundings

337 Thickness data were obtained using electromagnetic (EM) induction sounding that computes
338 the distance to the ice/water-interface by evaluating the amplitude and phase of a secondary EM
339 field induced by eddy currents in the seawater. With airborne measurements, the height of the
340 EM instrument above the air-snow surface is measured with a laser altimeter. Ice thickness is
341 then obtained from the difference of the EM distance measurement to the ice/water-interface and
342 the laser height of the snow [Haas *et al.*, 2009], hence ice thickness from the EM measurements
343 includes snow thickness.

344 The accuracy of the EM method is ± 0.1 m over level ice under typical summer conditions
345 [Haas *et al.*, 1997; Pfaffling *et al.*, 2007] with only small effects from melt ponds [Haas *et al.*,
346 1997; Eicken *et al.*, 2001]. The horizontal extent of induced eddy currents results in a
347 measurement footprint area of up to 3.7 times the instrument height above the water [Reid *et al.*,
348 2006]. The measured, unconsolidated ridge thickness can be less than 50% of its “true” thickness
349 [e.g., Haas and Jochmann, 2003], although the magnitude of this underestimate is uncertain. The
350 EM thickness distributions are most accurate with respect to modal thickness, while mean
351 thickness can still be used for relative comparisons between regions and years. Surveys were
352 performed with helicopters and fixed-wing aircraft using a towed sensor (“EM-Bird”) from
353 icebreakers and land bases in various regions of the eastern and western Arctic [Haas *et al.*,
354 2006; Haas *et al.*, 2008; Haas *et al.*, 2009; Haas *et al.*, 2010]. Surveys have generally been
355 performed in the April/May and August/September periods and data locations used in this paper
356 are shown in Figure 2.

357 4.3 Upward looking sonar and ice profiling sensors from moorings

358 Eleven moorings with upward looking sonars (ULS) deployed in Fram Strait and the
359 Greenland Sea (Figure 1b) by the Alfred Wegener Institute for Polar and Marine Research,

360 Bremerhaven, Germany acquired almost 25 station-years of data between 2002 and 2004 as a
361 contribution to the World Climate Research Programme's Arctic Climate System Study/Climate
362 and Cryosphere (ACSYS/CliC) Project. The ice draft data are available from the Unified Sea Ice
363 Thickness Climate Data Record as well as the National Snow and Ice Data Center web site with
364 data descriptions *Witte and Fahrback* [2005].

365 Sea ice draft data are available on the continental shelf of the Eastern Beaufort Sea for the
366 period April 1990 through September 2003 from Ice Profiling Sonar (IPS) instruments deployed
367 by H. Melling at the Institute for Ocean Sciences (IOS), Canada. Data are described in *Melling*
368 *and Riedel* [2008] and references therein. Sea ice draft data in the central Beaufort Sea for the
369 period 2003-2008 were acquired through the Beaufort Gyre Exploration Project (BGEP, A.
370 Proshutinsky, PI). The point data are available at the Woods Hole Oceanographic Institute web
371 site (<http://www.whoi.edu/beaufortgyre/data.html>).

372 *Melling and Riedel* [2004] estimate for their data an accuracy of ± 0.05 m draft for level ice.
373 Draft will be overestimated on average in rough ice. The ACSYS/CliC Workshop [*Steffen*, 2004]
374 on sea-ice thickness requires an accuracy of ± 0.05 m for draft for ULS and IPS and we use that
375 figure here for all ULS data. We acknowledge that NSIDC has been alerted to an error in the
376 way the bias correction was applied for the AWI data, but pending further clarification these data
377 are used assuming the above accuracy.

378 4.4 Upward Looking Sonar measurements from submarines

379 Submarines have traversed the Arctic regularly since 1958 measuring the draft of the
380 overhead sea ice using upward looking sonar (ULS). The processed and publicly available data
381 (archived at NSIDC and available as 50-km averages at the Unified Sea Ice Thickness Climate
382 Data Record) include 42 cruises from 1975 to 2000 covering 120,000 km of data. The cruises

383 took place between April and November, although most of the data were collected in late spring
384 (April-May) and in late summer-fall (August-October) [*Rothrock and Wensnahan, 2007*].

385 The draft data are produced for periods when the submarine was traveling in a straight line at
386 constant speed and depth. The basic data product is ice draft along the cruise track (Figure 2).
387 The data typically have a spacing of 1-8 m with a footprint size of 2-7 m depending on the
388 submarine depth. Data segments vary in length from a few to several hundred kilometers.

389 *Rothrock and Wensnahan [2007]* identify the following submarine ice draft measurement
390 errors: precision error; error in identifying open water (ice of zero draft); sound speed error; error
391 caused by sonar footprint size variations; error from uncontrolled gain and thresholds; error due
392 to vessel trim. There are also differences between analog versus digitally recorded data with
393 paper charts biased toward thicker ice by over 0.30 m due to their coarser temporal resolution.
394 The drafts are obtained from the "first return" or from the depth of the deepest ice within the
395 footprint. They estimated the overall bias due to this effect of the submarine ULS data from the
396 actual draft as +0.29 m with a standard deviation of ± 0.25 m. A recent paper [*Rodrigues, 2010*]
397 finds a bias based on the sonar beam width and ice roughness larger than that found by *Rothrock*
398 *and Wensnahan [2007]*. For this study we have corrected for the submarine draft bias of +0.29
399 m described in *Rothrock and Wensnahan [2007]*.

400 4.5 Pack-ice and fast-ice measurements from drill holes

401 Historical ice thickness data are available from the "Atlas of ice and snow of the Arctic Basin
402 and Siberian Shelf Seas" [*Romanov, 1995*]. This data set contains sea ice and snow Spring (mid
403 March – mid May) measurements collected during aircraft landings associated with the Soviet
404 Union's historical *Sever* airborne and North Pole drifting station programs. The High-Latitude
405 Airborne Annual Expeditions *Sever* took place in 1937, 1941, 1948-1952, and 1954-1993

406 [*Konstantinov and Grachev, 2000*]. The data set is derived from as few as 7 landings (1937) to
407 nearly pan-arctic coverage in the 1970s. The data set contains measurements of 23 parameters,
408 including a) ice thickness and snow depth on the runway and surrounding area, b) ridge,
409 hummock, and sastrugi dimensions and areal coverage and c) snow density. The data used in this
410 paper are a subset of those used to create the atlas “Morphometric Characteristics of Ice and
411 Snow in the Arctic Basin” (self-published by Ilya P. Romanov in 1993 and republished by
412 Backbone Publishing Company in 1995). Romanov provided these data to NSIDC in 1994 (see
413 <http://nsidc.org/data/g02140.html> for full description and data in ASCII format). In this paper we
414 use ice thickness data in the Spring from 1982 through 1986 (Figure 1b). The data were obtained
415 at sites adjacent to the aircraft landing areas (undisturbed ice).

416 We also use data from 51 coastal stations where sea ice thickness was measured monthly
417 through drill holes. The data represent thicknesses of the fast sea ice in the vicinity of the coastal
418 station, mostly first-year ice, undeformed by ridging or rafting. Monthly data are available for
419 1998-2009. The data were provided by the Arctic and Antarctic Research Institute, St.
420 Petersburg, Russia. Although these data and the data from the Romanov Atlas are unique, and
421 the accuracy of such direct measurements is likely less than 0.05 m, we cannot make a formal
422 statement regarding position error and accuracy.

423 5. **Methods**

424 All ice-draft data were converted to thickness as described above. In the following discussion,
425 model minus observed thickness values are referred to as residuals, and thus the residuals are
426 positive when the model overestimates the observed thickness. The observed data were monthly
427 averaged except for the ICESat data which are provided as ~2-month averages. Where model
428 results temporally overlapped the observed data, model ice thickness was extracted from the

429 nearest model grid point and averaged into monthly means. We recognize that the observational
430 data have very different spatial resolutions; moored instruments and drill holes produce point
431 data, while the ICESat data were processed using a 50-km Gaussian smoothing, and the Unified
432 Sea Ice Thickness Climate Data Record provides the statistical mean ice thickness at 50 km
433 intervals for the submarine ULS data. We chose to compare the observed data with the nearest
434 model grid point, an approach perhaps advantageous to models with finer resolution. For models
435 with coarse resolution, a 50-km weighted average, which is used by *Rothrock and Wensnahan*
436 [2007] might be advantageous. In this paper, we used the nearest model grid point to the
437 observed data, formed monthly averages of model and observational data (~2 months for
438 ICESat), and then computed residuals and correlations. This approach leads to consistent results,
439 described below, across data sets and models.

440 Record-length correlation coefficients and residuals were computed from the monthly time
441 series for each of the moored ULS and the 51 coastal stations data. Annual correlation
442 coefficients and residuals were computed for the each of the ICESat, airborne EM, Romanov
443 Atlas, and submarine data sets by averaging all data in the given year. Grand mean correlation
444 coefficients and residuals for each observational platform were computed by averaging all 25
445 ULS time series and from all 51 Coastal Station time series, and averaging all years for the
446 ICESat, airborne EM, Romanov Atlas, and submarine data. These differences should be kept in
447 mind in the following discussion.

448 To show the correlation coefficients and residuals, a modified Taylor Diagram [*Taylor, 2001*]
449 is used. In this diagram, the radial distance from the origin is the correlation coefficient ($r=1$ falls
450 on the unit circle) and the rotation angle (θ) is proportional to residuals with $\pm\pi$ corresponding
451 to residuals of ± 2 m (Figure 3).

452 A quantitative evaluation arises from the modified Taylor diagram where model performance
453 is proportional to the area swept by the radial “tip” $(1-r)$ rotated from zero to the residual (θ) .
454 The result, $|(1-r)\theta|$ is used to rank the model performance.

455 Linear regressions are used to obtain relationships between the observed and modeled time
456 series means and monthly means from the spatial data. We used annually averaged thickness for
457 ICESat and Romanov Atlas, monthly averages using the multiple locations for the airborne EM
458 and submarine ULS data, record-length means from the time series from moored ULS and the 51
459 Coastal Stations. Our purpose is to identify systematic biases in the simulations as a function of
460 observed thickness. Statistical differences among the correlations and residuals are not discussed
461 considering the different platforms, seasons, and instrument types. Our goal, rather, is to find
462 patterns of performance among the different models to guide model improvement.

463 **6. Comparisons between Observations and Model results**

464 **6.1 Drill holes from coastal stations and Romanov Atlas.**

465 The residuals from the Romanov drill hole data were averaged from 1982 through 1986 and
466 contoured using a color bar defined so that zero is white (Figure 4). All models, except for the
467 GSFC model, show positive residuals, typically larger in the eastern Siberian marginal seas
468 (East-Siberian and Chukchi Seas) than in the western seas (Kara and Laptev Seas).

469 **6.2 ICESat**

470 The residuals and correlations show that the models have a large scatter (Figure 5a). The UW,
471 ECCO2, and NPS models are correlated with data above 0.6 and have residuals less than +0.30
472 m. For GSFC, the correlation is larger than 0.6 and the residual is negative, less than -0.40 m.
473 The INMOM correlation is less than 0.5 and residual exceeds 0.40 m. (Post 2001 results from the
474 ORCA model were not available at the time of our analysis.)

475 **6.3 Airborne EM**

476 The model and EM correlations are all less than 0.5. All models underestimate ice thickness
477 except ECCO2 which has positive residuals (Figure 5b). Three models (GSFC, UW and NPS)
478 demonstrate clustering of the results and have almost identical residuals, approximately -0.50 m.
479 The negative residual occurs perhaps because the EM measurements include snow depth with the
480 ice thickness although they underestimate maximum ridge thickness.

481 **6.4 Moored ULS**

482 All six models have similarly moderate correlations with residuals less than 0.25 m (Figure
483 5c). ECCO2, UW and GSFC have higher correlations with the data, near 0.6, while INMOM,
484 NPS, and ORCA correlations are weaker. Of the six models, ECCO2 demonstrates the best
485 agreement with the moored ULS data. Three models, INMOM, NPS and ORCA, show similar
486 positive residuals. Two models, GSFC and UW, have negative, almost identical residuals.

487 **6.5 Submarine ULS**

488 ECCO2 has the highest correlation of ~0.7 in the suite of models with a residual of about
489 +0.17 m (Figure 5d). UW, ECCO2 and GSFC models have similar correlations of about ~ 0.7.
490 INMOM and NPS have positive residuals less than +0.70 m and correlations less than 0.6.
491 ORCA has the weakest correlation (0.48) and a negative residual of approximately -0.30 m.

492 **6.6 Coastal stations and Romanov Atlas**

493 All models overestimate thickness at the coastal stations except for GSFC (Figure5e). The
494 residuals are larger and more positive for the Romanov Atlas (symbols with squares in Figure
495 5e) except for GSFC which has a near zero residual for the station data and moderately negative
496 residual for the Romanov Atlas data. NPS has the highest correlation with both the datasets

497 although the residual for the Romanov Atlas data is large. GSFC shows the lowest correlation for
498 the station data, whereas ORCA has the weakest for the Romanov Atlas data.

499 **7. Basin-wide and regional model performance**

500 We focus on model performance with respect to the ULS data because of (i) their broad
501 spatial and temporal coverage, (ii) accuracy and biases of the measurements are relatively well
502 understood, and (iii), like model grid-points, ULS measurements are values at a point sampled
503 over time. The ULS data used here extend from 1990 through 2008 and cover the Beaufort Sea,
504 Fram Strait and the Greenland Sea.

505 Figure 6 portrays correlations and residuals for the data from each model and from the
506 individual moored ULS instruments. UW and ECCO2 show the smallest scatter of residuals
507 (Figure 6 a,b). Residuals for GSFC and NPS are larger (Figure 6 c,d). The largest absolute
508 residuals are from INMOM and ORCA with values approaching 2m (Figure 6 e,f). All models
509 exhibit large scatter of the correlations; there is no apparent relationship between the scatter of
510 the residuals and the correlations.

511 From Figure 6, the model performance clearly varies regionally. We next focus the analysis
512 on Fram Strait and the Greenland Sea and on the Beaufort Sea. Figure 7 combines correlations
513 and residuals for Fram Strait and the Greenland Sea (AWI moorings) and the Beaufort Sea (IOS
514 and BGEP moorings) for all models. The pattern exhibits a broader range of residuals for the
515 data acquired in Fram Strait/Greenland Sea compared to the Beaufort Sea. Typically the
516 residuals for the Beaufort Gyre are more positive and higher than these for the periphery of the
517 Beaufort Sea (Figure 7).

518 **8. Linear relationships**

519 The linear fit for the models and observations is shown in Figure 8 for a) satellite, b) airborne
520 EM, c) moored ULS, d) submarine ULS, e) Coastal Stations and f) Romanov Atlas. Grey
521 shading along the $y = x$ line indicates the accuracy of the measurements. In all but four cases,
522 the y-intercepts are greater than zero indicating positive residuals for thin ice. In all but three
523 cases the regression slopes are less than one. The regression lines cross $y=x$ at variable locations
524 with a mean of 2.2 m. For the satellite data (Figure 8a), INMOM, ECCO2, UW, and GSFC
525 overestimate thickness where it is measured less than 1m. INMOM, ECCO2 and UW
526 overestimate ice thinner than 2.0 - 2.5 m. NAME overlapped the satellite record only for 2004
527 and is omitted. For the airborne EM thicknesses (Figure 8b), all models strongly underestimate
528 thickness when the ice is thicker than 3.5 m. ORCA is omitted as it does not have enough data
529 for a meaningful comparison. For the moored ULS data (Figure 8c), GSFC strongly
530 underestimates ice thinner than 2m and NPS, GSFC, and UW overestimate thin ice. All models
531 except INMOM underestimate thick ice. For submarine ULS data (Figure 8d), all models
532 overestimate thickness when measurements are less than 2 to 3 m. All models underestimate ice
533 measured to be thicker than 4 m compared to submarine ULS.

534 Figure 8e shows that all models but NPS and GSFC overestimate near-shore ice thickness
535 when measured to be less than 1.5 m at the Coastal Stations (Figure 8e). GSFC is unable to
536 reproduce the range of the observed fast-ice measurements.

537 For the marginal seas (Romanov Atlas), INMOM, NPS, UW, and ORCA overestimate where
538 observed thickness is less than 3 m, and all models overestimate thickness where it is measured
539 to be less than 1 m (Figure 8f). (ECCO2 simulated 1992-2009 and does not overlap the Romanov
540 Atlas data.)

541 9. Discussion

542 The accuracy, systematic errors of the measurements and cross-platform biases discussed in
543 Section 4 should be taken into account when interpreting model results. Nevertheless, there are
544 consistent results among the models.

545 For all observational platforms, most model regressions have slopes less than one ($\bar{m} = 0.7$),
546 positive y-intercepts ($\bar{b} = 0.9$), and cross the $y=x$ line (perfect fit) at a mean observed
547 thicknesses of 2.1 m. The regressions indicate that thin ice is overestimated and thick ice is
548 underestimated although each model varies around the 2.1 m mean crossing point (range -3.4 to
549 7.7). Overestimating thin ice is particularly evident with respect to the satellite data (Figure 8a).
550 For the thickest ice (airborne EM and submarine ULS), which is generally the most deformed, all
551 models underestimate thickness (Figure 8 a, b, d). There is thus a consistent pattern across
552 platforms and across models to overestimate thin ice and underestimate thick ice. Below we
553 investigate possible reasons for this bias.

554 The correlations are computed from multiple data sets that include different seasonal and
555 spatial variability. For example, correlations should always be higher if the seasonal cycle is
556 included compared to the correlations for just one season. This may explain why the modified
557 Taylor diagrams suggest that the models perform well compared to the moored ULS (Figure 5).

558 Model performance is a clearly geographically dependent. Figures 5 and 6 demonstrate that
559 the models as a group perform better in the Beaufort Sea than in other areas of the Arctic Ocean.
560 The comparison with the IOS and BGEP moorings shows a smaller range of residuals than the
561 other datasets. Scatter of the residuals for ULS measurements in Fram Strait and the Greenland
562 Sea is larger than in the Beaufort Sea and substantial (Figure 7). Ice conditions in Fram Strait
563 depend on local forcing as well as on conditions “upstream” in the Arctic Ocean making
564 predictions for Fram Strait ice export dependent on many factors. However, the fact that the

565 models do well in the central basin but not in Fram Strait and the Greenland Sea may suggest
566 regional issues in Fram Strait are driving the poor performance there.

567 The poorest correlations are with the ice measured from the Airborne EM and the Romanov
568 Atlas for the marginal Siberian seas. The residuals for the Airborne EM dataset are mostly
569 negative and for the Romanov Atlas mostly positive and are larger than for the other data (Figure
570 5).

571 The models demonstrate reasonably good agreement with the coastal station data, which
572 partly overlap the area of the Romanov Atlas measurements (Figures 5 and 8). The residuals for
573 the coastal data have moderate scatter, however there is a positive bias of ~50 cm (Figure 5e).
574 The bias may be because the station data represent only level sea ice whereas the model data are
575 the cell-averaged level and ridge ice thicknesses. Note that AOMIP models do not have fast ice
576 (motionless ice).

577 There are three aspects of the model biases. First, the biases tend to be smaller for the data
578 which include several complete seasonal cycles (moored ULS and station data) and larger for the
579 data covering only part of the year (satellite, Airborne EM, submarine ULS and Romanov Atlas).
580 Since the latter mostly cover the ice melting period (spring to fall), we speculate that this may be
581 related to model deficiencies in the thermodynamics of ice melting. The ice thickness threshold
582 of 2.1 m, which in our analysis discriminates the positive and negative model bias, is the
583 commonly accepted thickness distinguishing undeformed first- and multi-year Arctic sea ice
584 [WMO, 1985]. This may indicate insufficient melting of first-year and the excessive melting of
585 multi-year ice in the models. In our study we did not find any systematic differences between
586 models with Semtner and energy-conserving thermodynamics.

587 The mean residual we found after averaging the annual residuals for the submarine ULS
588 (Figure 5d) is 0.12 m. Recall that the submarine data were corrected for the 0.29 m bias reported
589 by *Rothrock and Wensnahan* [2007]. As a group, the AOMIP models do well, overestimating
590 submarine ULS by 0.12 m. We note that the Louvain-la-Neuve (LIM3) model [*Vancoppenolle et*
591 *al.*, 2009a] underestimated submarine draft observations converted to thickness by -0.55 ± 1.04 .
592 However, similar to our results, they obtained positive model bias for the thin ice and a negative
593 bias for the thick ice. *Vancoppenolle et al.* [2009b] performed sensitivity study of ice
594 thermodynamics to the sea ice salinity and demonstrated a 0.30 m reduction in the model bias
595 when the salt evolution model is used instead of constant or prescribed varying salt profiles.

596 Second, the model biases indicate a regional dependency. Our analysis shows small residuals
597 in the Beaufort Sea and the central Arctic Ocean (moored and submarine ULS data) and an
598 increase of the positive residuals on the Siberian Shelf (station data and Romanov Atlas).
599 *Rothrock et al.* [2003] and *Vancoppenolle et al.* [2009a], comparing model results with
600 submarine ULS, obtained a persistent pattern of model biases with positive values in the
601 Beaufort Sea, north of Greenland and towards the Alaskan and East-Siberian Shelves, and with
602 negative values in the Arctic Transpolar Drift and towards Fram Strait. *Wilchinsky et al.* [2004]
603 found a similar pattern in their simulations and demonstrated that using sliding friction in sea ice
604 rheology can reduce the biases.

605 The third aspect is the interannual variability in the models and data. Given the errors in
606 atmospheric temperature, humidity and radiation fields used to force the models, we would
607 expect large model biases for individual years even though the overall long-term biases could be
608 moderate. Most of the available Arctic ice thickness data represent a few “samples” per year
609 when aggregated to a monthly time scale. This poses a large statistical uncertainty of the

610 analysis. In addition, since the periods of the data collection varied from year to year, this
611 introduces aliasing in the time series, making interpretation of the interannual variability
612 difficult.

613 10. Summary

614 Sea ice thickness from six AOMIP coupled models is compared with thickness across the
615 Arctic basin from a) satellites, b) airborne EM, c) moored ULS in Fram Strait, Greenland Sea
616 and the Beaufort Gyre (ULS, IPS), d) submarine ULS across the central basin, and e) drill holes
617 through fast along coastal Siberia and within the ice pack. The linear relationship between
618 models and the different data shows that all models generally overestimates ice thinner than 2.1
619 m and underestimate the ice thicker than 4.0 m. This is a systematic error consistent among the
620 models and is likely problematic for forecasting open water as well as in long term forecasts
621 where the role of multi-year ice is critical. We speculate that this error may be attributed to the
622 deficiencies in simulating ice melting. We did not find any systematic error with respect to the
623 type of ice thermodynamics used in the models.

624 There is a significant scatter of the model biases with respect to the different observational
625 platforms, which could be partly related to the observational systematic errors. The models agree
626 best with the moored ULS data. The model skill in simulating sea ice thickness varies from
627 region to region. Taken together, the models simulate the ice thickness in the Beaufort Gyre
628 better than in Fram Strait and the Greenland Sea. Some of the observed scatter is also due to
629 inconsistencies between different observational methods and data products. Averaging over all
630 observational data sets, the correlations and smaller differences from observed thickness are
631 better from the ECCO2 and UW models.

632

633 **Acknowledgements**

634 This research is supported by the National Science Foundation Office of Polar Programs
635 covering awards of AOMIP collaborative research projects: ARC-0804180 (MJ), ARC-0804010
636 (AP), ARC-0805141 (WM), ARC080789 and ARC0908769 (JZ). Travel support to attend
637 AOMIP meetings and publications fees for YA, IA, deCuevas, SH, RK, RL, and AN were
638 provided by OPP project ARC-0804010. C. Haas is grateful for support with data acquisitions
639 through the Alfred Wegener Institute in Germany and various EU projects. This research is also
640 supported by the Russian Foundation of Basic Research, Projects 09-05-00266 and 09-05-01231.
641 At the National Oceanography Centre Southampton this study was funded by the UK Natural
642 Environment Research Council as a contribution to the Marine Centres' Strategic Research
643 Programme Oceans2025. The NOCS-ORCA simulations were undertaken as part of the
644 DRAKKAR collaboration [*Barnier et al.*, 2006]. NOCS also acknowledges the use of UK
645 National High Performance Computing Resource.

646

647 **Reference list**

648 Adcroft, A., and J.-M. Campin (2004), Rescaled height coordinates for accurate representation of
649 free-surface flows in ocean circulation models, *Ocean Modelling*, 7 (3-4), 269--284.
650 Adcroft, A., C. Hill, and J. Marshall (1997), The representation of topography by shaved cells in
651 a height coordinate model, *Mon. Weather Rev.*, 125 (9), 2293—2315.
652 Alexandrov, V., S. Sandven, J. Wahlin, and O. M. Johannessen (2010), The relation between sea
653 ice thickness and freeboard in the Arctic, *The Cryosphere*, 4, 373–380, [www.the-](http://www.the-cryosphere.net/4/373/2010/)
654 [cryosphere.net/4/373/2010/](http://www.the-cryosphere.net/4/373/2010/) doi:10.5194/tc-4-373-2010.

655 Antonov, J.I., R.A. Locarnini, T.P. Boyer, A.V. Mishonov, and H.E. Garcia (2006), *World*
656 *Ocean Atlas 2005*, chap. Volume 2: Salinity, p. 182pp, NOAA Atlas NESDIS 62, U.S.
657 Government Printing Office, Washington, D.C.

658 Barnier B., Madec G., Penduff, T., Molines, J. M., Tréguier, A. M., Beckmann, A., Biastoch, A.,
659 Boning, C., Dengg, J., Gulev, S., Le Sommer, J., Rémy, E., Talandier, C., Theetten, S.,
660 Maltrud, M., Mc Lean, J. and B de Cuevas (2006), Impact of partial steps and momentum
661 advection schemes in a global ocean circulation model at eddy permitting resolution. *Ocean*
662 *Dyn.* 56, 543–567. DOI 10.1007/s10236-006-0082-1.

663 Bitz, C.M., J. Fyfe, and G. Flato (2002), Sea ice response to wind forcing from AMIP models, *J.*
664 *Climate*, 15, 522-536

665 Blanke B. and P. Delecluse (1993), Variability of the tropical Atlantic Ocean simulated by a
666 general circulation model with two different mixed-layer physics. *J. Phys. Oceanogr.* 23,
667 1363-1388.

668 Blumberg A., and G. L. Mellor, (1987), A description of a three-dimensional coastal ocean
669 circulation model. In *Three-Dimensional Coastal Ocean Models*, N. S. Heaps (Ed.), 1-16,
670 American Geophysical Union, Washington, DC

671 Bourke, R. H., and R. P. Garrett (1987), Sea ice thickness distribution in the Arctic Ocean, *Cold*
672 *Reg. Sci. Technol.*, 13(3), 259 – 280.

673 Bourke, R. H., and R. G. Paquette (1989), Estimating the thickness of sea ice, *J. Geophys. Res.*,
674 94, 919 – 923

675 Brodeau L., Barnier B., Penduff T., Treguier A.M. and S. Gulev (2001), An ERA-40 based
676 atmospheric forcing for global ocean circulation models. *Ocean Modelling*, 31, 88-104.

677 Brydon D., S. San, R. Bleck (1999), A new approximation of the equation of state for seawater,
678 suitable for numerical ocean models. *J. Geophys. Res.*104, C1., 1537-1540.

679 Dai A., and K.E. Trenberth (2002), Estimates of freshwater discharge from continents: latitudinal
680 and seasonal variations. *Journal of hydrometeorology*, 3, 660-687.

681 Daru, V., and C. Tenaud (2004), High order one-step monotonicity-preserving schemes for
682 unsteady compressible flow calculations, *J. Comput. Phys.*, 193 (2), 563--594,
683 doi{<http://dx.doi.org/10.1016/j.jcp.2003.08.023>}.

684 Eicken, H., W.B. Tucker III, D.K. Perovich (2001), Indirect measurements of the mass balance
685 of summer Arctic sea ice with an electromagnetic induction technique, *Ann.Glaciol.*, 33, 194-
686 200.

687 Fichefet T. and M. A. Morales Maqueda (1997), Sensitivity of a global sea ice model to the
688 treatment of ice thermodynamics and dynamics. *J. Geophys. Res.* 102, 12609-12646.

689 Flato, G.M. and CMIP contributors (2004), Sea-ice climate and sensitivity as simulated by global
690 climate models, *Climate Dynamics*, 23: 229-241

691 Flato G.M., Hibler, W.D. III (1995), Ridging and strength in modeling the thickness distribution
692 of Arctic sea ice. *J. Geophys Res.*, 100:18,611–18,626.

693 Fox-Kemper, B., and D. Menemenlis (2008), Can large eddy simulation techniques improve
694 mesoscale rich ocean models?, in *Ocean Modeling in an Eddying Regime*, edited by M. Hecht
695 and H. Hasumi, pp. 319--338, AGU, Washington, D.C.

696 Gaspar P., Grégoris Y. and J. M. Lefevre (1990), A simple eddy-kinetic-energy model for
697 simulations of the ocean vertical mixing: tests at station Papa and long-term upper ocean study
698 site. *J. Geophys. Res.* 95, 16,179-16,193.

699 Gerdes, R., and C. Köberle (2007), Comparison of Arctic sea ice thickness variability in IPCC
700 Climate of the 20th Century experiments and in ocean–sea ice hindcasts, *J. Geophys.*
701 *Res.*, *112*, C04S13, doi:10.1029/2006JC003616

702 Gloersen, P., Campbell, W. J., Cavalieri, D. J., Comiso, J. C., Parkinson, C. L., and Zwally, H. J.
703 (1992), Arctic and Antarctic sea ice, 1978-1987: Satellite passive-microwave observations and
704 analysis: Washington, NASA Scientific and Technical Information Program SP-511, 290 p.

705 Haas, C., and P. Jochmann (2003), Continuous EM and ULS thickness profiling in support of ice
706 force measurements. In Proceedings of the 17th International Conference on Port and Ocean
707 Engineering under Arctic Conditions, POAC '03, Trondheim, Norway, vol. 2, edited by S.
708 Loeset, B. Bonnemaire, and M. Bjerkas, pp. 849–856, Department of Civil and Transport
709 Engineering, Norwegian University of Science and Technology NTNU, Trondheim, Norway.

710 Haas, C., S. Gerland, H. Eicken, and H. Miller (1997), Comparison of sea-ice thickness
711 measurements under summer and winter conditions in the Arctic using a small electromagnetic
712 induction device. *Geophysics*, *62*(3), 749–757.

713 Haas, C., Hendricks, S., Doble, M.(2006), Comparison of the sea ice thickness distribution in the
714 Lincoln Sea and adjacent Arctic Ocean in 2004 and 2005, *Annals of glaciology*,*44*, 247-252.

715 Haas, C., S. Hendricks, H. Eicken, and A. Herber (2010), Synoptic airborne thickness surveys
716 reveal state of Arctic sea ice cover, *Geophys. Res. Lett.*, *37*, L09501,
717 doi:10.1029/2010GL042652.

718 Haas, C., J. Lobach, S. Hendricks, L. Rabenstein, and A. Pfaffling (2009), Helicopter-borne
719 measurements of sea ice thickness, using a small and lightweight, digital EM system, *J. Appl.*
720 *Geoph.*, *67*(3), 234–241, 2009, doi:10.1016/j.jappgeo.2008.05.005.

721 Haas, C., A. Pfaffling, S. Hendricks, L. Rabenstein, J.-L. Etienne, and I. Rigor (2008), Reduced
722 ice thickness in Arctic Transpolar Drift favors rapid ice retreat, *Geophys. Res. Lett.*, 35,
723 L17501, doi:10.1029/2008GL034457.

724 Hakkinen, S. and C.A. Geiger (2000), Simulated low frequency modes of circulation in the
725 Arctic Ocean, *J. Geophys. Res.*, 105, 6549-6564.

726 Hakkinen, S., and G. L. Mellor (1992), Modeling the seasonal variability of the coupled Arctic
727 ice-ocean system, *J. Geophys. Res.*, 97, 20,285 –20,304

728 Hibler, W.D., III (1979), A dynamic thermodynamic sea ice model. *J. Phys. Oceanogr.* 9, 815-
729 846.

730 Hibler, W. D., (1980), Modeling a Variable Thickness Sea Ice Cover. *Mon. Wea. Rev.*, **108**,
731 1943-1973. doi: 10.1175/1520-0493

732 Hibler, W. D., and K. Bryan (1987), A Diagnostic Ice Ocean Model, *J.Phys. Oceanogr.*, 17, 987-
733 1015.

734 Holland, D.M. (2000), Merged IBCAO/ETOPO5 Global Topographic Data Product. National
735 Geophysical Data Center (NGDC), Boulder CO.

736 Holland, D., Holloway, G., F. E. Dupont, E. Golubeva, S. Hakkinen, E. Hunke, M. Jin, M. Karcher,
737 F. Kauker, M. Maltrud, M. A. Morales Maqueda, W. Maslowski, G. Platov, D. Stark, M. Steele,
738 T. Suzuki, J. Wang, and J. Zhang (2007), *J. Geophys. Res.*, v.112, C04S03, doi:
739 10.1029/2006JC003642.

740 Hunke, E. C. (2001), Viscous-plastic sea ice dynamics with the evp model: Linearization
741 issues. *J. Comp. Phys.*, **170**, 18-38.

742 Hunke, E.C. and C.M. Bitz (2009), Age characteristics in a multidecadal arctic sea ice
743 simulation. *J. Geophys. Res.*, 114, C08013, doi:10.1029/2008JC005186.

744 Hunke, E., and M. Holland (2007), Global atmospheric forcing data for Arctic ice-ocean
745 modeling, *J. Geophys. Res.*, 112, C06S14, doi:10.1029/2006JC003.

746 Jackett, D. R., and T. J. McDougall (1995), Minimal adjustment of hydrographic profiles to
747 achieve static stability, *J. Atmos. Oceanic Technol.*, 12 (2), 381—389.

748 Johnson, M., S. Gaffigan, E. Hunke, and R. Gerdes (2007), A comparison of Arctic Ocean sea
749 ice concentration among the coordinated AOMIP model experiments, *J. Geophys. Res.*, 112,
750 C04S11, doi:10.1029/2006JC003690.

751 Kalnay, E., M. Kanamitsu, R. Kistler, W. Collins, D. Deaven, L. Gandin, M. Iredell, S. Saha, G.
752 White, J. Woollen, Y. Zhu, M. Chelliah, W. Ebisuzaki, W. Higgins, J. Janowiak, K. C. Mo, C.
753 Ropelewski, J. Wang, A. Leetmaa, R. Reynolds, Roy Jenne, Dennis Joseph (1996). The
754 NCEP/NCAR 40-Year Reanalysis Project. *Bulletin of the American Meteorological*
755 *Society* **77** (3): 437–471

756 Kochergin V. P. (1987), Three-Dimensional Prognostic Models, in *Coastal Ocean Models*, Ed.
757 by N. Heaps (AGU, Coastal and Estuarine Science, Vol. 4, 841–849.

758 Konstantinov, Yu. B., K. I. Grachev. 2000. *High-latitude Airborne Expeditions Sever (1937,*
759 *1941 – 1993)*. Gidrometeoizdat Publishing House, St. Petersburg, Russia, 176 pp

760 Kwok, R., and D.A. Rothrock (2009), Decline in Arctic sea ice thickness from submarine and
761 ICESat records: 1958:2008. *Geophys. Res. Lett.*, V. 36, L15501, doi:10.1029/2009GL039035,
762 2009

763 Kwok, R., G. F. Cunningham, M. Wensnahan, I. Rigor, H. J. Zwally, and D. Yi (2009), Thinning
764 and volume loss of the Arctic Ocean sea ice cover: 2003 – 2008, *J. Geophys. Res.*, 114,
765 C07005, doi:10.1029/2009JC00531

766 Kwok, R., G. F. Cunningham, H. J. Zwally, and D. Yi (2007), Ice, Cloud, and land Elevation
767 Satellite (ICESat) over Arctic sea ice: Retrieval of freeboard, *J. Geophys. Res.*, 112, C12013,
768 doi:10.1029/2006JC003978

769 Kwok, R., E. Hunke, W. Maslowski, D. Menemenlis, and J. Zhang (2008), Variability of sea ice
770 simulations assessed with RGPS kinematics. *J. Geophys. Res.*, 131, C11012.

771 Kwok, R., H. J. Zwally, and D. Yi (2004), ICESat observations of Arctic sea ice: A first look.
772 *Geophys. Res. Lett.*, 31, L16401, doi:10.1029/2004GL020309.

773 Large W. G. and S.G. Yeager (2004), Diurnal to decadal global forcing for ocean and sea-ice
774 models: The data sets and flux climatologies. NCAR technical note: NCAR/TN-460+STR,
775 NCAR, 105pp.

776 Large, W. G., J. C. McWilliams, and S. C. Doney (1994), Oceanic vertical mixing: a review and
777 a model with nonlocal boundary layer parameterisation, *Rev. Geophys.*, 32, 363-403.

778 Laxon, S., N. Peacock, and D. Smith (2003), High interannual variability of sea ice thickness in
779 the Arctic region, *Nature*, 425, 947 – 950.

780 Leith, C. E. (1996), Stochastic models of chaotic systems, *Physica D*, 98, 481—491.

781 Lévy M., Estublier A. and G. Madec (2001), Choice of an advection scheme for biogeochemical
782 models. *Geophys Res Lett.* 28, 3725–3728. DOI 10.1029/2001GL012947.

783 Lindsay, R. W. (2010), Unified Sea Ice Thickness Climate Data Record, Polar Science Center,
784 Applied Physics Laboratory, University of Washington, psc.apl.washington.edu/sea_ice_cdr,
785 digital media.

786 Locarnini, R. A., A. V. Mishonov, J. I. Antonov, T. P. Boyer, and H. E. Garcia (2006), *World*
787 *Ocean Atlas 2005*, chap. Volume 1: Temperature, 182pp, NOAA Atlas NESDIS 62, U.S.
788 Government Printing Office, Washington, D.C.

789 Losch, M., D. Menemenlis, P. Heimbach, J.-M. Campin, and C. Hill (2010), On the formulation
790 of sea-ice models. part 1: effects of different solver implementations and parameterizations,
791 *Ocean Modelling*, 33, 129—144.

792 Madec, G. (2006), NEMO reference manual, ocean dynamics component: NEMO-OPA.
793 Preliminary version. Note du Pole de modélisation, Institut Pierre-Simon Laplace (IPSL),
794 France, 27, ISSN No. 1288-1619.

795 Marshall, J., A. Adcroft, C. Hill, L. Perelman, and C. Heisey (1997), A finite-volume,
796 incompressible Navier-Stokes model for studies of the ocean on parallel computers, *J.*
797 *Geophys. Res.*, 102 (C3), 5753—5766.

798 Maslowski, W., and W. Lipscomb (2003), High resolution simulations of Arctic sea ice, 1979 –
799 1993, *Polar Res.*, 22, 67 – 74

800 Maslowski, W., J. Clement Kinney, D. C. Marble, J. Jakacki, (2008) In: Ocean Modeling in an
801 Eddyding Regime, M. W. Hecht and H. Hasumi, eds. Geophysical Monograph Series, Volume
802 177, 350 pp.

803 Maslowski, W., D. Marble, W. Walczowski, U. Schauer, J. L. Clement, and A. J.
804 Semtner (2004), On climatological mass, heat, and salt transports through the Barents Sea and
805 Fram Strait from a pan-Arctic coupled ice-ocean model simulation, *J. Geophys. Res.*, 109,
806 C03032, doi:10.1029/2001JC001039.

807 Maslowski, W., B. Newton, P. Schlosser, A. Semtner, and D. Martinson (2000), Modeling recent
808 climate variability in the Arctic Ocean, *Geophys. Res. Lett.*, 27, 3743 – 3746

809 Melling, H., and D.A.Riedel (2004), Draft and movement of pack ice in the Beaufort Sea: a time-
810 series presentation April 1990 – August 1999. Canadian Technical Report of Hydrography and
811 Ocean Sciences 238. 331pps.

812 Mellor, H., and D.A. Riedel (2008), Ice Draft and Ice Velocity Data in the Beaufort Sea, 1990-
813 2003. Boulder, Colorado USA: National Snow and Ice Data Center. Digital media.

814 Mellor, G.L, S. Hakkinen, T. Ezer, and R. Pazan, (2002), A generalization of a sigma coordinate
815 ocean model and an intercomparison of model vertical grids, in 'Ocean Forecasting: Theory
816 and Practice', N. Pinardi and J.D.Woods, eds., Springer-Verlag, 55-72. Pub.

817 Mellor, G.L. and L.H. Kantha (1989), An ice-ocean coupled model, *J. Geophys. Res.*, 94, 10937-
818 10954.

819 Mellor, G.M. and T. Yamada (1974), A hierarchy of turbulence closure models for planetary
820 boundary layer, *J. Atmos. Sci.*, 31, 1791-1806.

821 Mellor, G.L. and T. Yamada (1982), Development of a turbulence closure model for geophysical
822 fluid problems, *Rev. Geophys.*, 20, 851-875.

823 Menemenlis, D., J.M. Campin, P. Heimbach, C. Hill, T. Lee, A. Nguyen, M. Schodlok, H. Zhang
824 (2008), ECCO2: High resolution global ocean and sea ice data synthesis, *Mercator Ocean
825 Quarterly Newsletter*, 31, 13—21.

826 Moshonkin S.N., G.V. Alekseev, A.V. Bagno, A.V. Gusev, N.A. Diansky, and V.B. Zalesny
827 (2011), Numerical modeling of the 20th century variability of the North Atlantic-Arctic
828 Ocean-Bering Sea circulation. *Russian Journal of Numerical Analysis and Mathematical
829 Modelling*. Vol. 26, Issue 2, (in press).

830 Nguyen, A. T., D. Menemenlis, and R. Kwok (2009), Improved modeling of the Arctic halocline
831 with a subgrid-scale brine rejection parameterization, *J. Geophys. Res.*, 114, C11014.

832 Nguyen, A.T., D. Menemenlis, and R.Kwok (2011), Arctic ice-ocean simulation with optimized
833 model parameters: approach and assessment. *J. Geophys. Res.* (in press)

834 Onogi, K., J. Tsutsui, H. Koide, M. Sakamoto, S. Kobayashi, H. Hatsushika, T. Matsumoto,
835 N. Yamazaki, H. Kamahori, K. Takahashi, S. Kadokura, K. Wada, K. Kato, R. Oyama, N. M.
836 T. Ose, and R. Taira (2007), The jra-25 reanalysis, *J. Meteor. Soc. Japan*, 85 (3), 369—43.
837 Pacanowski, R.C., and A. Gnanadesikan (1998), Transient response in a Z-level ocean model
838 that resolves topography with partial cells, *Monthly Weather Review*, 126, 3248-3270.
839 Parkinson, C. L., and W. M. Washington (1979), A large scale numerical model of sea ice, *J.*
840 *Geophys. Res.* 84, 311-337.
841 Payne, R.E. (1972), Albedo of the sea surface. *J. Atmos. Sci.*, 29, 959-970.
842 Penduff, T., J. Le Sommer, B. Barnier, A.-M. Treguier, J.-M. Molines, and G. Madec (2007),
843 Influence of numerical schemes on current-topography interactions in 1/4° global ocean
844 simulations, *Ocean Sci.*, 3, 509-524.
845 Rodrigues, J. (2011), Beamwidth effects on sea ice draft measurements from U.K. submarines,
846 *Cold Regions science and Techn.*, 65, 160-171.
847 Semtner, A.J. (1976), A model for the thermodynamic growth of sea ice in numerical
848 investigation of climate. *J. Phys. Oceanogr.* 6, 376-389.
849 Pfaffling, A., C. Haas, and J. Reid (2007), A direct helicopter EM sea ice thickness inversion,
850 assessed with synthetic and field data, *Geophysics*, 72, F127-F137.
851 Prather, M.C. (1986), Numerical advection by conservation of second-order moments. *J.*
852 *Geophys. Res.* 91, 6671-6681.
853 Rasmusson, E.M. and K. Mo (1996) Large scale atmospheric moisture cycling as evaluated from
854 NMC global analysis and forecast products, *J. Climate*, 9, 3276-3297.
855 Reid, J. E., A. Pfaffling, J. Vrbancich (2006), Airborne electromagnetic footprints in 1D earths,
856 *Geophysics*, 71(2), G63-G72, doi:10.1190/1.2187756.

857 Romanov, I.P. (1995), In: Tunik, A. (Ed.), Atlas of Ice and Snow of the Arctic Basin and
858 Siberian Shelf Seas. Backbone Publishing Company. 277 pp.

859 Rothrock, D. A., and M. Wensnahan (2007), The accuracy of sea ice drafts measured from U.S.
860 Navy submarines, *J. Atmos. Oceanic Technol.*, 24, 1936– 1949, doi:10.1175/JTECH2097.1.

861 Rothrock, D. A., Y. Yu, and G. A. Maykut (1999), Thinning of the Arctic sea-ice cover,
862 *Geophys. Res. Lett.*, 26(23), 3469 – 3472, doi:10.1029/1999GL010863.

863 Rothrock, D. A., D. B. Percival, and M. Wensnahan (2008), The decline in arctic sea-ice
864 thickness: Separating the spatial, annual, and interannual variability in a quarter century of
865 submarine data, *J. Geophys. Res.*, 113, C05003, doi:10.1029/2007JC004252.

866 Rothrock, D. A., J. Zhang, and Y. Yu (2003), The arctic ice thickness anomaly of the 1990s: A
867 consistent view from observations and models, *J. Geophys. Res.*, 108(C3), 3083,
868 doi:10.1029/2001JC001208.

869 Semtner, A.J. (1976), A model for the thermodynamic growth of sea ice in numerical
870 investigation of climate. *J. Phys. Oceanogr.* 6, 376-389.

871 Smith, R.D., J. K. Dukowicz, and R. C. Malone, (1992), Parallel ocean general circulation
872 modeling. *Physica D*, 60, 30–6.

873 Smith, R.D. and P. R. Gent, Eds., (2002), Reference manual for the Parallel Ocean Program
874 (POP): Ocean component of the Community Climate System Model (CCSM2.0 and 3.0).

875 Smith, W. H. F., and D. T. Sandwell (1997), Global sea floor topography from satellite altimetry
876 and ship depth soundings, *Science*, 277 (5334), 1956—1962.

877 Steele, M., et al. (2001), PHC: A global ocean hydrography with a highquality Arctic Ocean, *J.*
878 *Clim.*, 14, 2079 – 2087

879 Steffen, K. (ed.) (2004), Workshop on Sea-Ice Thickness Measurements from Moored Ice-
880 Profiling Sonars: Calibration, Data Processing and Application, Arctic Climate System Study
881 and Climate and Cryosphere Project, Informal Report No. 15/2004.

882 Taylor, K. E. (2001), Summarizing multiple aspects of model performance in a single diagram, *J.*
883 *Geophys. Res.*, 106(D7), 7183-7192

884 Thorndike, A. S., D. S. Rothrock, G. A. Maykut and R. Colony (1975), The thickness
885 distribution of sea ice. *J. Geophys. Res.*, **80**, 4501-4513

886 Timmermann, R., H. Goose, G. Madec, T. Fichefet, C. Etche, and V. Duliere (2005), On the
887 representation of high latitude processes in the ORCA-LIM global coupled sea ice-ocean
888 model, *Ocean Model.*, 8, 175–201.

889 Untersteiner, N. (1961), On the mass and heat budget of Arctic sea ice, *Arch. Meteor. Geophys.*
890 *Bioklimatol., Ser. A.* 12. 151-182.

891 Vancoppenolle M., T. Fichefet and H. Goosse (2009), Simulating the mass balance and salinity
892 of Arctic and Antarctic sea ice.2. Sensitivity to the ice salinity processes *Ocean Modelling* 27,
893 54-69.

894 Vancoppenolle, M., T. Fichefet, H. Goosse, S. Bouillon, G. Madec, and M. A. Morales Maqueda
895 (2009a), Simulating the mass balance and salinity of Arctic and Antarctic sea ice. 1. Model
896 description and validation, *Ocean Modelling*, 27 (1–2), 33–53,
897 doi:doi:10.1016/j.ocemod.2008.10.005.

898 Volodin E. M., N. A. Dianskii, and A. V. Gusev (2010), Simulating Present-Day Climate with
899 the INMCM4.0 Coupled Model of the Atmospheric and Oceanic General Circulations.
900 *Izvestiya, Atmospheric and Oceanic Physics*, ISSN 0001-4338. Vol. 46, No. 4, 2010. 414-431.

901 Wadhams, P. (1990), Evidence for thinning of the Arctic ice cover north of Greenland, *Nature*,
902 345,795-797.

903 Wadhams, P., and N. R. Davis (2000), Further evidence of ice thinning in the Arctic
904 Ocean, *Geophys. Res. Lett.*, 27(24), 3973–3975, doi:10.1029/2000GL011802

905 Walsh, J.E., Crane, R.G. (1992), A comparison of GCM simulations of Arctic climate. *Geophys.*
906 *Res. Lett.* 19, 29–32

907 Wilchinsky, A.V., and D.L.Feltham (2004), Dependence of sea ice yield-curve shape on ice
908 thickness. *J.Phys.Ocean.*, 34, 2852-2856.

909 Winsor, P. (2001), Arctic sea ice thickness remained constant during the 1990s, *Geophys. Res.*
910 *Lett.*, 28(6), 1039 – 1041

911 Witte, H., and E. Fahrbach (2005), AWI moored ULS data, Greenland Sea and Fram Strait,
912 1991-2002. Boulder, CO: National Snow and Ice Data Center/World Data Center for
913 Glaciology. Digital media.

914 World Meteorological Organization (1985), WMO sea-ice nomenclature, terminology, codes and
915 illustrated glossary, WMO/DMM/BMO 259-TP-145, Secretariat of the WMO, Geneva.

916 Yaglom, A.M. and B.A.Kader (1974), Heat and mass transfer between a rough wall and
917 turbulent flow at high Reynolds and Pcelet numbers, *J.Fluid Mech.*, 62, 601-623.

918 Yakovlev N.G. (2009), Reproduction of the Large-Scale State of Water and Sea Ice in the Arctic
919 Ocean in 1948–2002: Part I. Numerical Model. *Izvestiya, Atmospheric and Oceanic Physics*,
920 ISSN 0001-4338. Vol. 45, No. 3, 2009, 357-371.

921 Zhang, J. (2005), Warming of the arctic ice-ocean system is faster than the global average since
922 the 1960s, *Geophys. Res. Lett.*, 32.

923 Zhang, J. and W.D. Hibler (1997), On an efficient numerical method for modeling sea ice
924 dynamics, *J. Geophys. Res.*, *102*, 8691–8702.

925 Zhang, J., and M. Steele (2007), The effect of vertical mixing on the Atlantic water layer
926 circulation in the Arctic Ocean, *J. Geophys. Res.*, *112*, C04S04, doi:10.1029/2006JC003732.

927 Zhang, J., and D. Rothrock (2001), A thickness and enthalpy distribution sea-ice model, *J. Phys.*
928 *Oceanogr.*, *31*, 2986-3001.

929 Zhang, J., and D.A. Rothrock (2003), Modeling global sea ice with a thickness and enthalpy
930 distribution model in generalized curvilinear coordinates, *Mon. Wea. Rev.*, *131*(5), 681–697.

931 Zhang, J., and D.A. Rothrock (2005), The effect of sea-ice rheology in numerical investigations
932 of climate, *J. Geophys. Res.*, *110*, C08014, doi:10.1029/2004JC002599.

933 Zhang, Y., W. Maslowski, and A.J. Semtner (1999), Impact of mesoscale ocean currents on sea
934 ice in high resolution Arctic ice and ocean simulations, *J. Geophys. Res.*, *104*(C8), 18,409-
935 18,430.

936

937 **Figure Captions**

938 **Figure 1.** (a) ICESat data extent for the February-March and October-December 2004 – 2008
939 campaigns. (b) Locations of ULS in Fram Strait and the Greenland Sea (AWI, red), Beaufort Sea
940 (BGEP, blue; IOS, green), Romanov (1995) landing data from subset of High-Latitude Airborne
941 Annual (Sever) Expeditions (dark red dots), and 51 coastal fast ice stations (dark grey).

942

943 **Figure 2.** Locations of the airborne EM thickness data (dark) and submarine ULS ice draft data
944 (light).

945 **Figure 3.** Taylor diagram modified so the correlation coefficient is the radial distance from the
946 center. The rotation angle is proportional to the residual (model minus observed thickness) where
947 ± 2 m rotates to $\pm\pi$ with larger residuals rotated away from the positive x-axis. A correlation
948 coefficient of 0.6 is marked by the dashed green circle and residuals of 30 and 75 cm are marked.

949 **Figure 4.** Residual sea ice thickness from the Romanov Atlas data (stations in Figure 1) from
950 1982 through 1986 for (a) UW, (b) NPS, (c) GSFC, (d) INMOM, and (e) ORCA. No ECCO2
951 model results overlap with the Romanov data. Blue color identifies where model overestimates
952 thickness (UW, NPS, INMOM, ORCA) and red color denotes underestimate (GSFC).

953 **Figure 5.** Correlations and residuals for models and (a) ICESat, (b) airborne EM, (c) moored
954 ULS (d) submarine ULS, (e) 51 coastal stations and Romanov Atlas (with squares).

955 **Figure 6.** Correlations and residuals for moored ULS data. UW and ECCO2 have smaller
956 residuals compared to other models. GSFC and NPS have larger residuals. INMOM and ORCA
957 have the largest residuals with some approaching 2 m. AWI instrument data are in red, IOS in
958 green, and BGEP in blue.

959 **Figure 7.** Correlations and residuals for moored ULS data from (a) Fram Strait and the
960 Greenland Sea (AWI) and (b) Beaufort Sea (IOS, BGEP). The models simulate better the data
961 from the Beaufort Sea compared to Fram Strait and the Greenland Sea. Colors identifying each
962 model are the same as in Figure 6.

963 **Figure 8.** Linear fit between observed and model thickness from (a) satellites, (b) airborne EM,
964 (c) moored ULS, (d) submarine ULS, (e) coastal stations, and (f) Romanov Atlas. Each axis limit
965 is set from the maximum observed using the particular platform. Measurement accuracy is
966 shown by the width of the grey area behind the black $y = x$ line. A width of 10 cm is used for the
967 coastal station data and Romanov Atlas.

970 **Table 1.** Model Configuration and Selected Parameters^a

	GSFC	ECCO2	INMOM	NOCS	NAME	UW
Domain	regiona	regional	regional	global	regional	regional
Resolution	1	15-22km	0.25°	3-6 km	9 km	6-75 km
Ice Δt	0.35° - 045° 720 s	600 s	3600 s	7200 s	2800s	1152 s
Vertical coordinate	z	z	σ	z	z	z
Vertical levels	26	50	27	64	45	30
Minimum depth	25m	5m	5m	6.06	10	5m
Bering Strait	Restore d	Not restored	open	Fully represented in global domain	open	open
Equation of state	Mellor	Jackett and McDougal, 1995	Brydon et al., 1999	Jackett & McDougall (1995)	UNESCO	UNESCO
Vertical	MY2.5	KPP, no	Monin and	TKE	Pacanowsk	KPP

mixing		double diffusion	Obukhov, (Kochergin, 1987)	(Gaspar <i>et al.</i> (1990), Blanke & Delecluse (1993))	i and Philander	
Tracer advection	Lin et al 1994 Piecewise parabolic	7 th order monotonicity-preserving (Direct space time with flux limiter) [Daru and Tenaud, 2004]	Central diff.	TVD (Lévy <i>et al.</i> 2001)	Central diff.	Central diff.
Momentum advection	centered	vector invariant	Central diff.	EEEN (Barnier <i>et al.</i> 2006)	Central diff.	Central diff.
Salinity	5	Function of surface S	4	6	4	4
Thickness categories ^d	2: ice and no ice	8 (7 for ice and 1 for open water)	1	1	2: mean grid cell ice thickness	12

					or open water	
Advection	Centered moment Upwind A+D	Centered 2 nd order	MPDATA	Prather, 2 nd order, 2 nd moment conserving	Central diff.	Central diff.
Dynamics ^e	General ized viscous	Viscous plastic	EVP	VP	Viscous plastic	Teardrop plastic rheology, LSR solver
<i>Albedos</i>						
Melting snow	Cold snow - 0.85 0.78 – melting snow	0.8085	0.7-0.8 (surface temperature dependent)	0.5-0.65 (clear sky, snow thickness dependent)		0.70
Cold ice	0.74	0.7	0.1-0.65 (ice thickness dependent)	0.1-0.72 (clear sky, ice thickness dependent)	0.73	0.75

Melting ice	0.7	0.7060	0.1-0.575 (ice thickness and surface temperature dependent)	0.1-0.5 (clear sky, ice thickness dependent)		0.64
Ocean	0.1	0.1556	0.1	0.06	.10	0.1
<i>Surface Momentum Exchange Coefficients</i>						
Atmos.-ice ^g	1.4E-3	1.14 x 10 ⁻³	2.75 x 10 ⁻³	1.63 x 10 ⁻³	1.1 x 10 ⁻³	Surface BL
Ice-Ocean	BL model	5.4 x 10 ⁻³	5.5 x 10 ⁻³	5.0 x 10 ⁻³	5.5 x 10 ⁻³	Cw=0.005 5

971 ^aSee AOMIP web site for additional details (<http://www.whoi.edu/AOMIP>)

972 Table 2. ICESat campaign periods

Laser	Campaign year	Period	Operational Days
2a	2003	Sep 24 – Nov18	55
2b	2004	Feb 17 - Mar 21	34
3a	2004	Oct 03 – Nov 08	37
3b	2005	Feb 17 – Mar 24	36
3d	2005	Oct 21 – Nov 24	35
3e	2006	Feb 22 – Mar 27	34
3g	2006	Oct 25 – Nov 27	34
3h	2007	Mar 12 – Apr 14	34
3i	2007	Oct 02 – Nov 05	37
3j	2008	Feb 17 – Mar 21	34

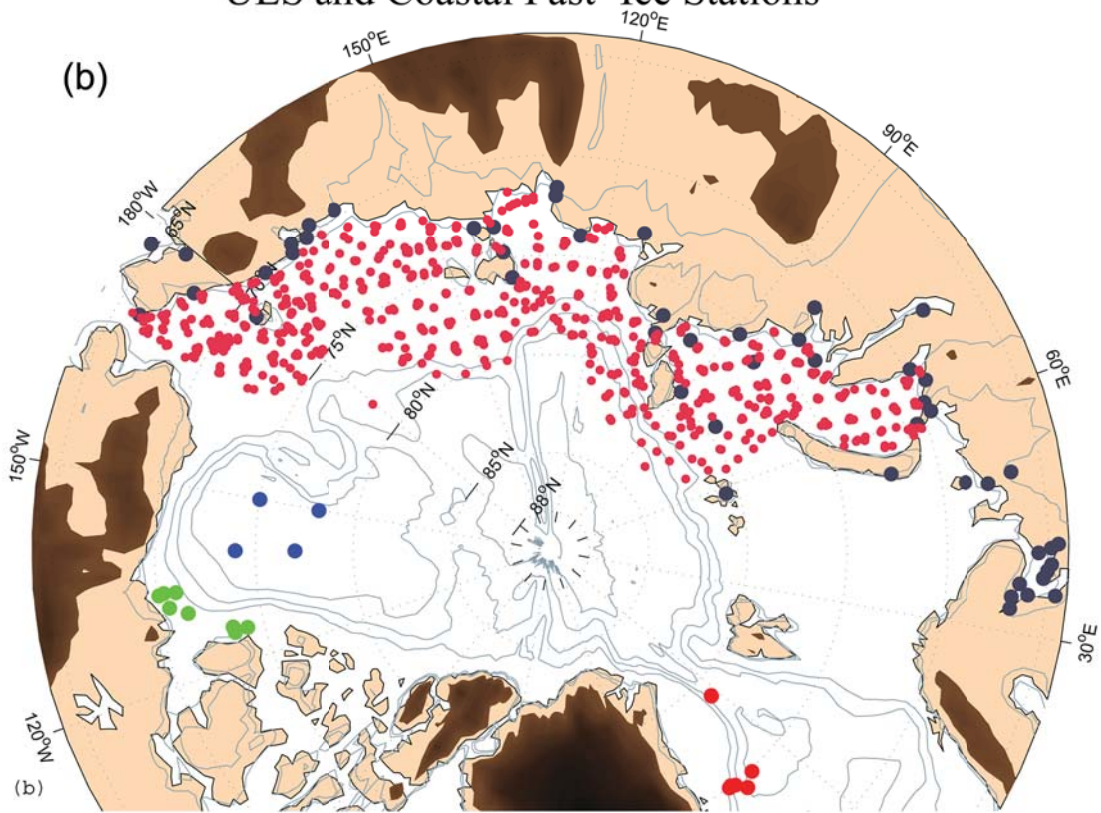
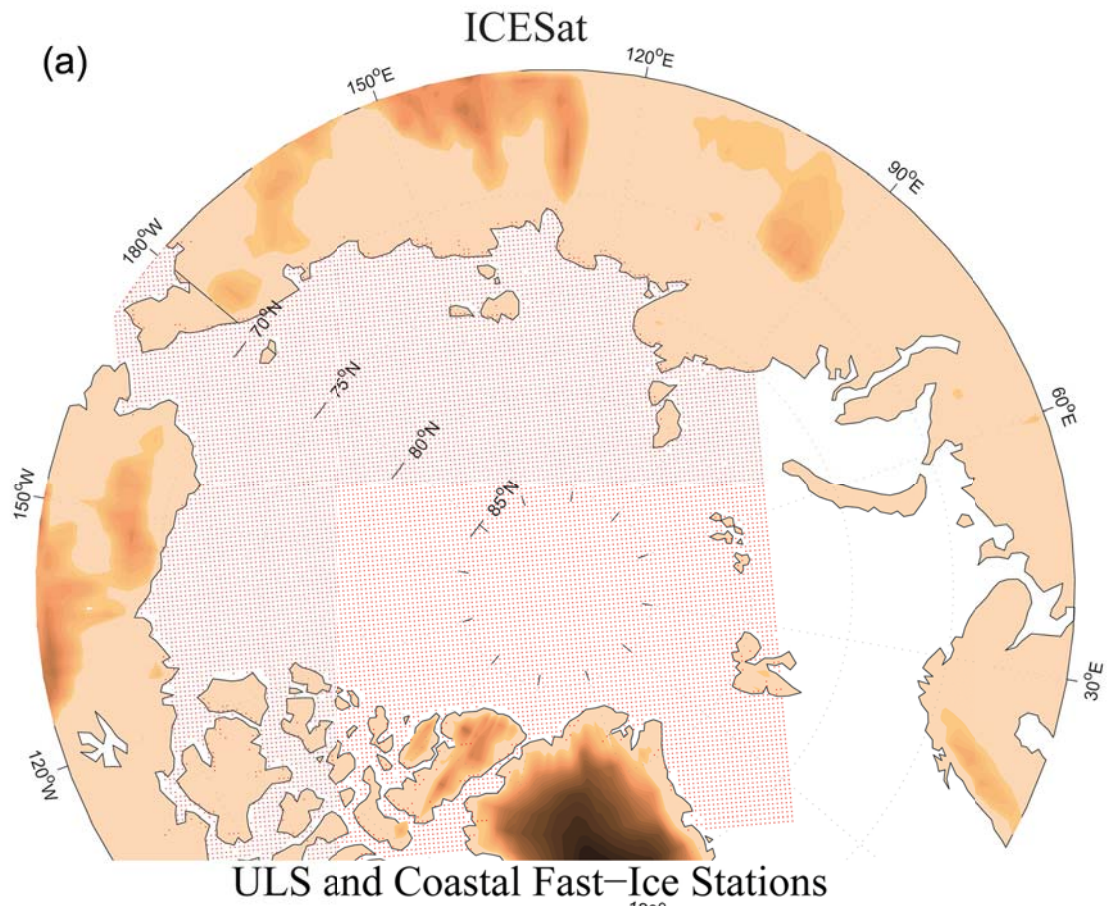


Figure 1

Submarine and Airborne EM Stations

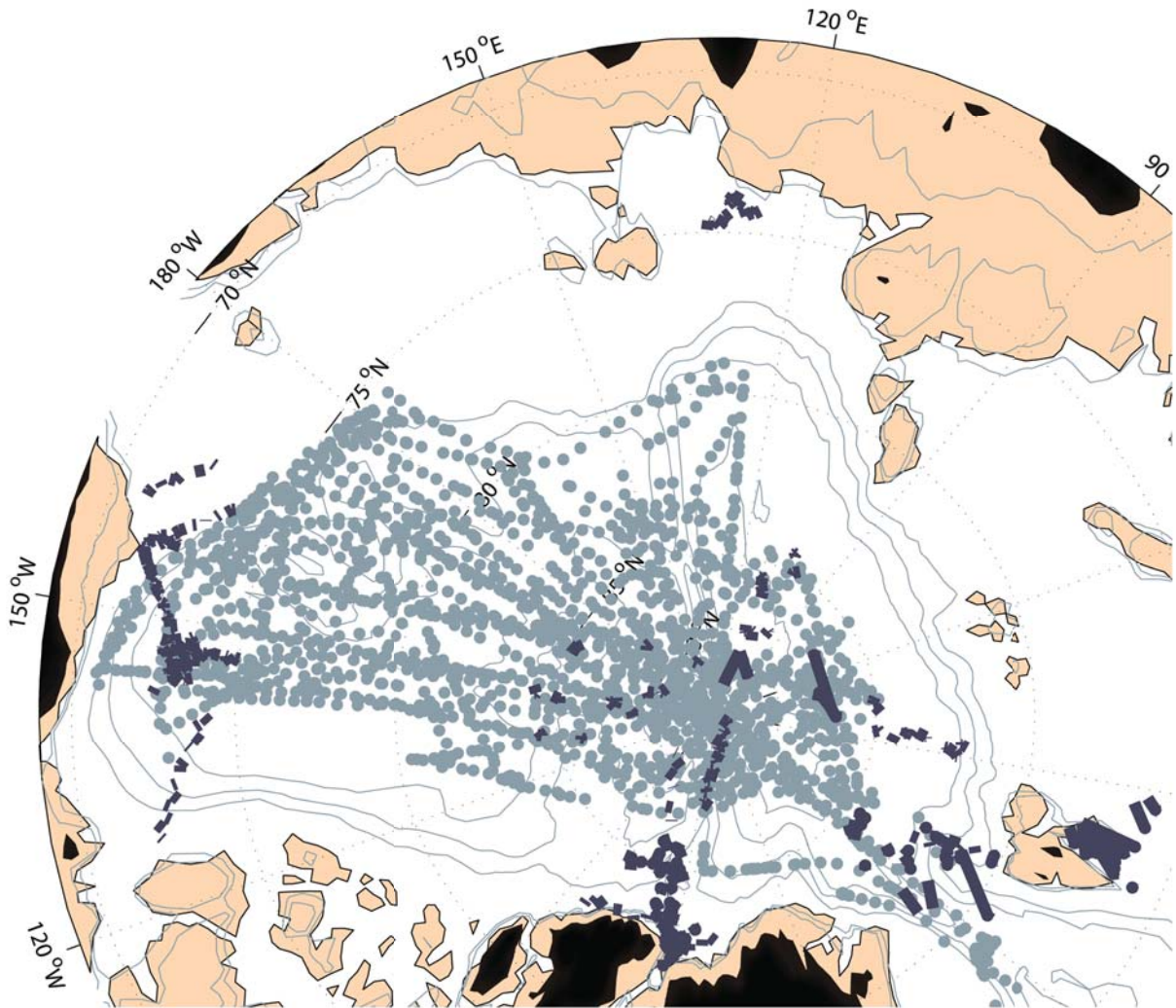


Figure 2

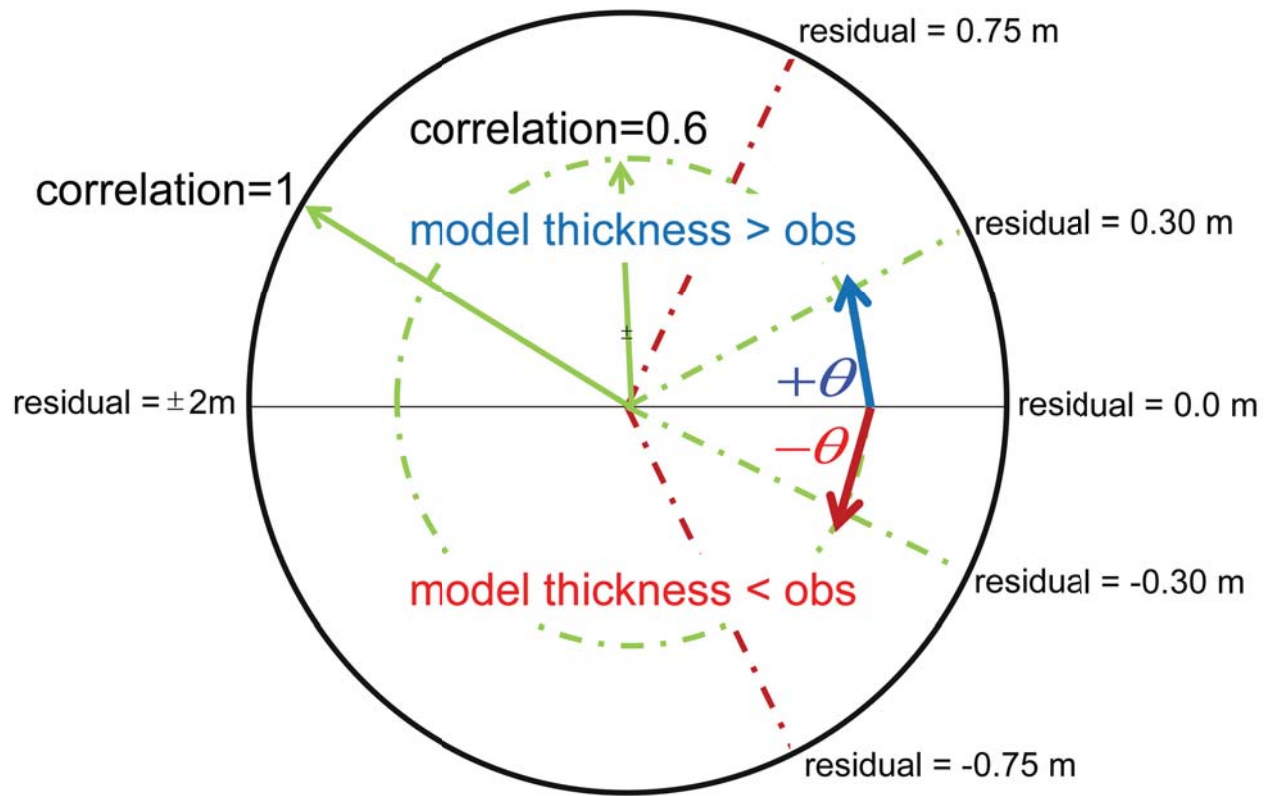


Figure 3

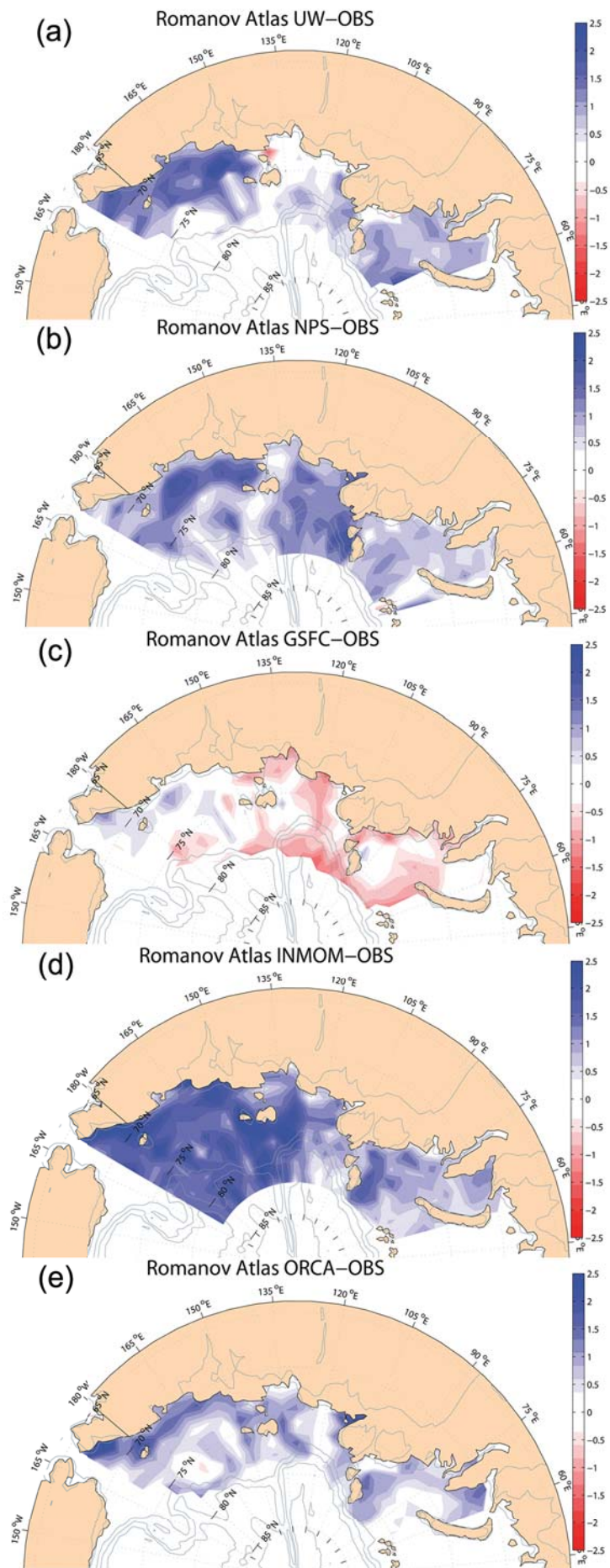


Figure 4

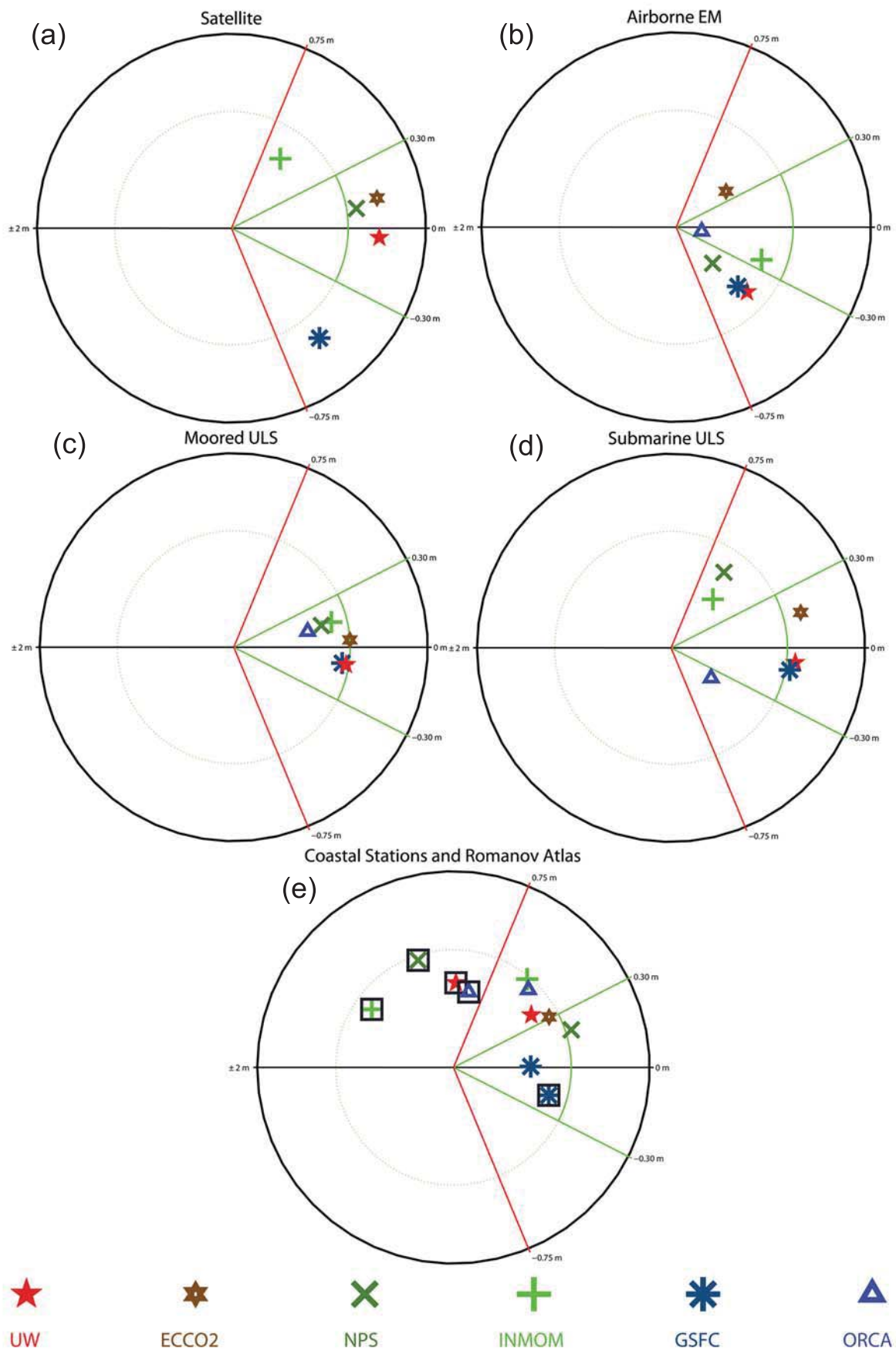


Figure 5

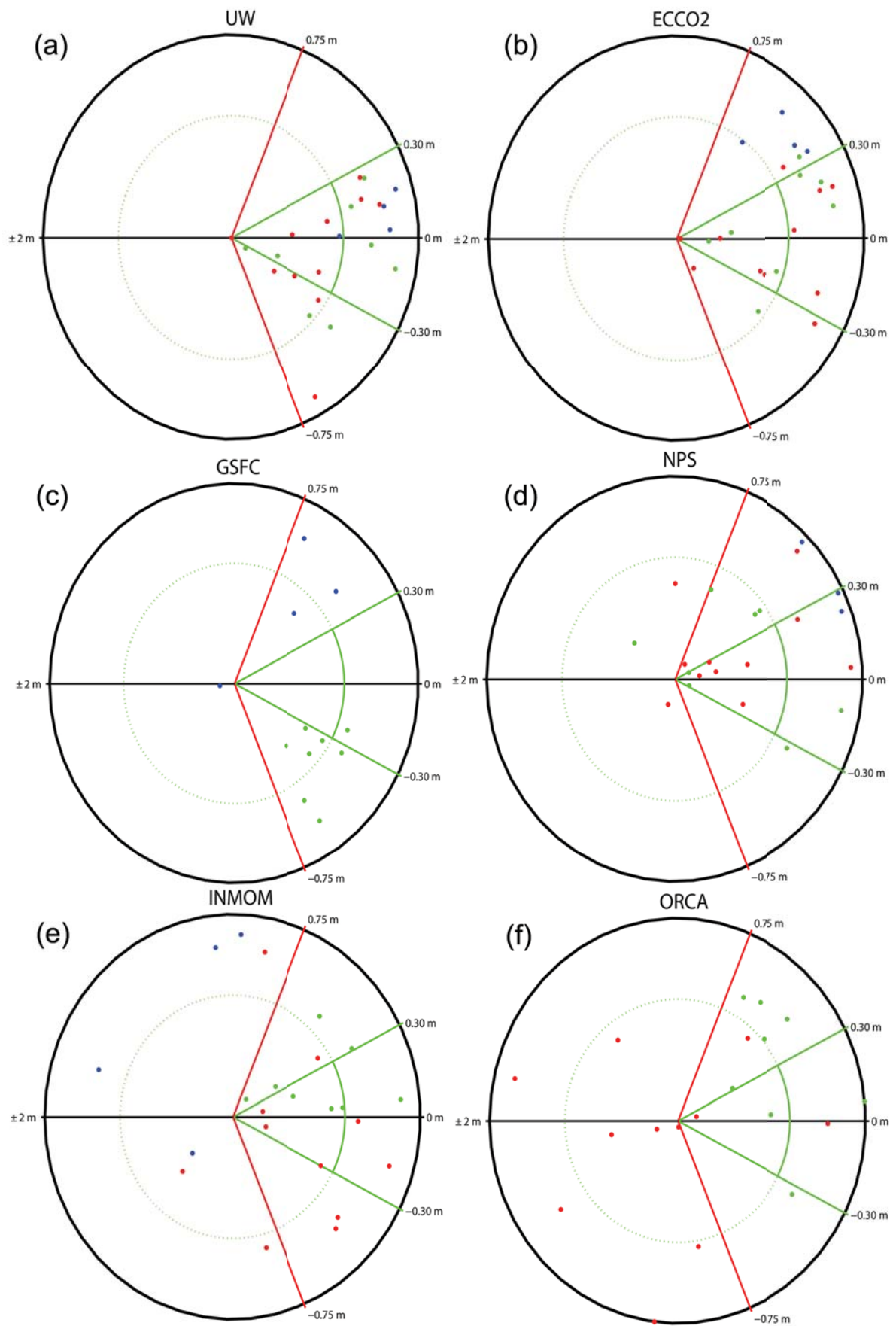


Figure 6

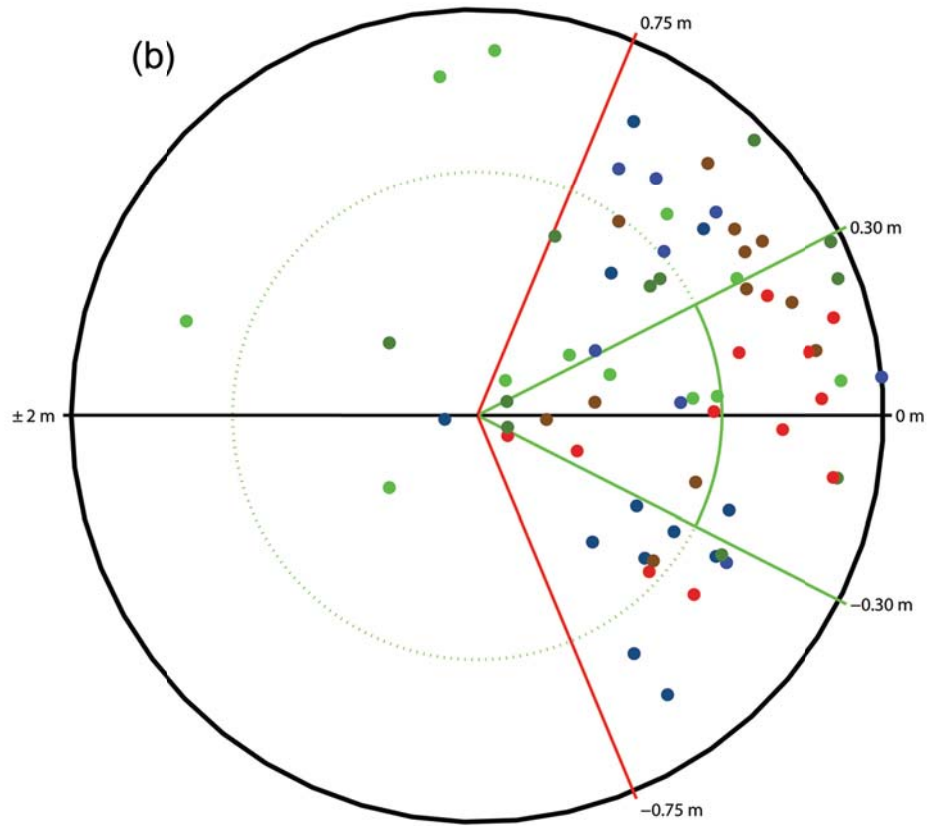
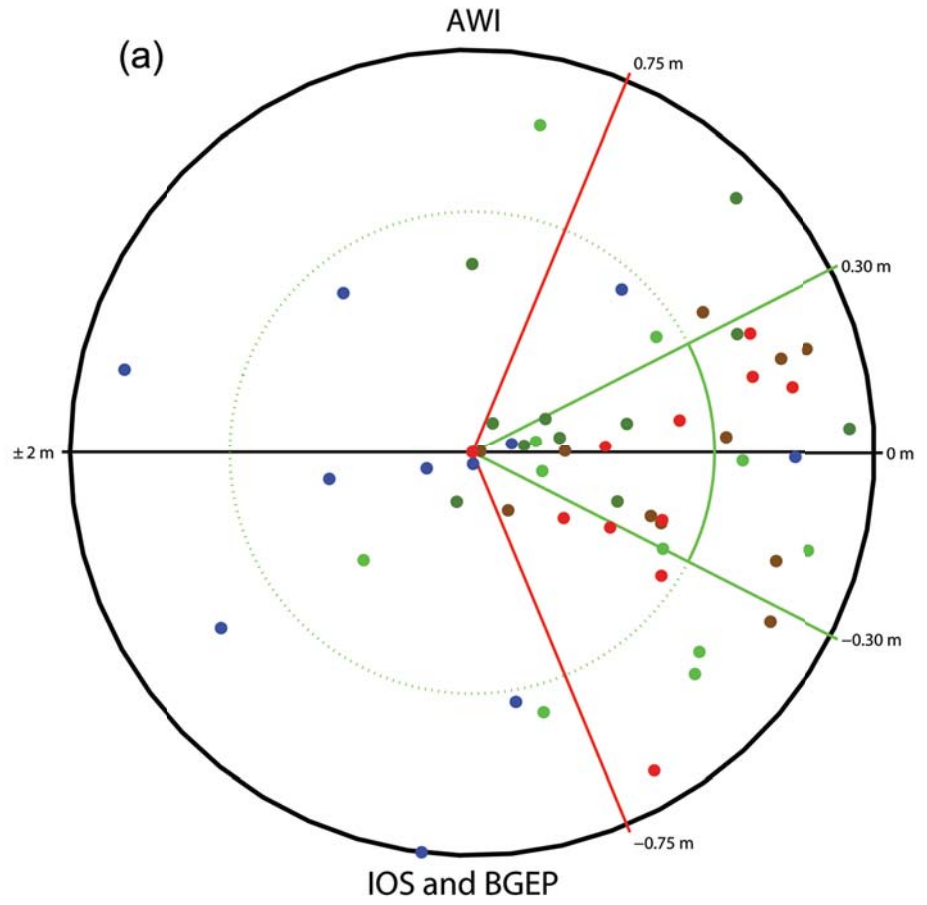


Figure 7

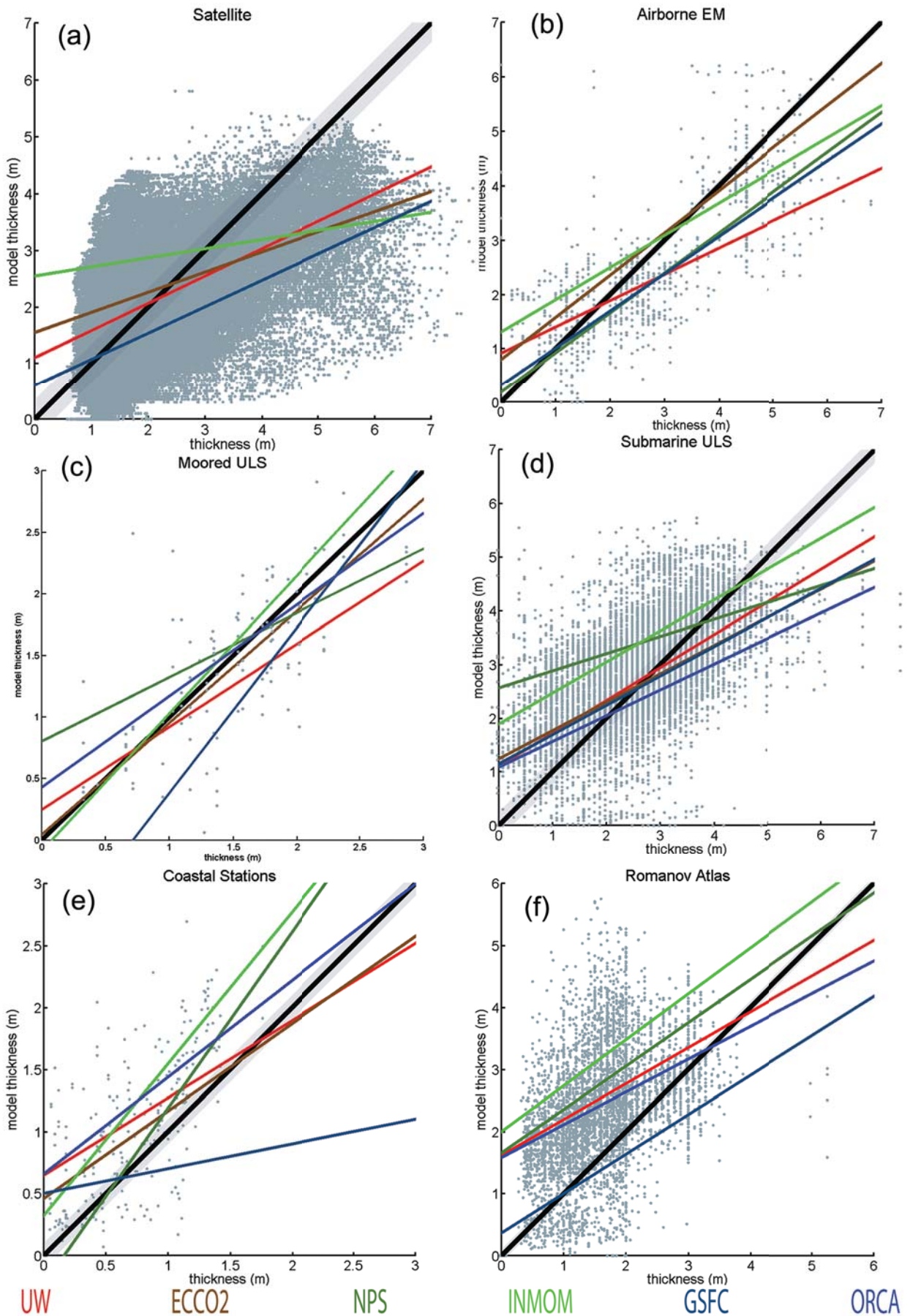


Figure 8